THE ASTROPHYSICAL JOURNAL, 190:609–630, 1974 June 15

MODELS OF ASYMPTOTIC-GIANT-BRANCH STARS

P. R. WOOD
Mount Stromlo and Siding Spring Observatory, Research School of Physical Sciences,
Australian National University
Received 1973 July 17; revised 1974 January 11

ABSTRACT

The static structure and dynamical behavior of the envelopes of four 0.9 $M_\odot$ asymptotic-giant-branch stars are described. It is found that in a model of luminosity $\log L/L_\odot = 3.42$ the envelope pulsates steadily in the first-overtone mode. The full-amplitude pulsational properties of this model agree well with those of a Mira variable of the same period. Three more-luminous models ($\log L/L_\odot = 3.60$, 3.85, and 4.14) all pulsate in the fundamental mode while simultaneously undergoing violent relaxation oscillations. Mass loss occurs from the models of luminosity $\log L/L_\odot = 3.60$ and 4.14. The models which execute envelope relaxation oscillations have properties which resemble those of some of the symbiotic stars. A distinct outward-moving shell which forms in the two most luminous models suggests a connection with planetary-nebula ejection.

Subject headings: combination spectra — interiors, stellar — late-type stars — long-period variables — mass loss — pulsation

I. INTRODUCTION

It is generally believed that planetary-nebula shells are ejected from red-giant stars (Abell and Goldreich 1966), probably from the asymptotic giant branch (Salpeter 1971; Faulkner 1972). In particular, the Mira variables and the symbiotic stars have been suggested as the immediate precursors of planetary nebulae (Paczyński and Ziołkowski 1968; O'Dell 1966; Abell and Goldreich 1966 and references therein). The most plausible mechanisms proposed for the ejection of matter from red giants are: (1) dynamical instabilities in the envelope (Roxburgh 1967; Paczyński and Ziołkowski 1968); and (2) ejection of the envelope via radiation pressure (Faulkner 1970; Finzi and Wolf 1971; Sparks and Kutter 1972). Since the onset of both these mechanisms is caused by an increase in luminosity, the ejection will almost certainly occur during the luminosity pulse associated with a thermal relaxation oscillation of the helium-burning shell. It is assumed here that the red giant is on the asymptotic giant branch (AGB) and that the time required to complete the ejection is shorter than the duration of the luminosity increase resulting from the shell relaxation oscillation.

Theoretical studies of the nonlinear dynamical behavior of the envelopes of red-giant stars have been reported by Keeley (1970*b*) and Smith and Rose (1972). Keeley found that two of his models were very unstable and some mass loss occurred from one of the models, while Smith and Rose found that a small amount of mass loss occurred during an envelope relaxation oscillation of a 0.856 $M_\odot$ star. The aim of the calculations reported here is to study the dynamical behavior of the envelope of a 0.9 $M_\odot$ star as the luminosity increases on the AGB and to seek mass loss on the scale required for the production of planetary nebulae. Since the models represent stars in the quiescent shell-burning phase of evolution, the core mass will be slightly larger than the core mass of a star of the same luminosity during a relaxation oscillation of the helium-burning shell.

Section II(*a*) describes the structure of the hydrostatic starting models used in the dynamical calculations. Particular emphasis is placed on the change in the structure with increasing luminosity on the AGB. Model 1 ($\log L/L_\odot = 3.42$) and model 4 ($\log L/L_\odot = 4.14$) are described in detail while the other models have intermediate characteristics. Kamijo (1962), Paczyński (1969), and Keeley (1970*a*) have previously discussed the structure of hydrostatic models of red giant stars. Section II(*b*) discusses the evolution of AGB stars in the H-R diagram. In the following sections the results of the dynamical calculations are presented and compared with observation. A summary is given in § VIII. Details of the envelope physics and numerical methods employed are given in the Appendix.

II. STATIC MODELS

a) Detailed Structure

Static envelope models with abundances $(X, Z) = (0.68, 0.02)$ were generated as hydrostatic solutions of the hydrodynamic program described in the Appendix. A stellar evolution program was used to obtain the mass, luminosity, and radius of the core of each model. The cores contained both hydrogen- and helium-burning shells, as required for stars on the AGB. Since in each case the hydrogen-burning shell is the predominant luminosity source in the core, the models represent stars in the quiescent shell-burning phase between flashes of the unstable helium-burning shell (Schwarzschild and Härm 1967). Table 1 gives the parameters of the four hydrostatic models while figure 1 shows the cores of the four models in the (luminosity, core-mass)-plane, together with the cores of double-shell-source models of other authors.

Between models 1 and 4, the radius of the envelope increases with luminosity while the mass in the

TABLE 1

HYDROSTATIC MODELS OF ASYMPTOTIC-GIANT-BRANCH STARS

Parameter	Model 1	Model 2	Model 3	Model 4
M_r/M (H shell)....	0.6512	0.7014	0.7503	0.8015
M_r/M (He shell)....	0.6215	0.6793	0.7352	0.7963
M_1/M.....	0.9826	0.9729	0.9386	0.9157
log $(L/L_\odot)$.....	3.415	3.604	3.846	4.142
log $(L_H/L_\odot)$.....	3.227	3.436	3.790	4.119
log $(L_{He}/L_\odot)$.....	2.909	3.041	1.659	1.546
log $(L_{grav}/L_\odot)$.....	2.063	2.338	2.953	2.832
log T_{eff} $(\tau = \frac{2}{3})$....	3.422	3.419	3.412	3.440
$R/R_\odot$.....	250	310	425	536

NOTE.—The mass fractions specified for the shells are those at which the rate of nuclear energy generation is a maximum. M_1/M is the mass fraction at the outer edge of the region of efficient convection.

envelope decreases. As a result, the mean pressure and density in the envelope decrease as shown in figure 2. The increasing luminosity also causes the density distribution within the envelope to change, and in model 4 the density increases outward throughout much of the envelope to a maximum at the outer edge of the convection-ionization zone. The result of this change is that while the mass in the envelope is distributed quite uniformly with the radius in model 1, most of the mass in the envelope of model 4 is concentrated in a shell centered around the density maximum at $\sim 420\ R_\odot$ (see fig. 3). Figure 3 shows that radiation pressure becomes increasingly important in the interior of the envelope as the luminosity increases. At the high luminosities represented by model 4, a static AGB star envelope consists of a shell of convective material supported to a large extent by the pressure of the enclosed sphere of radiation.

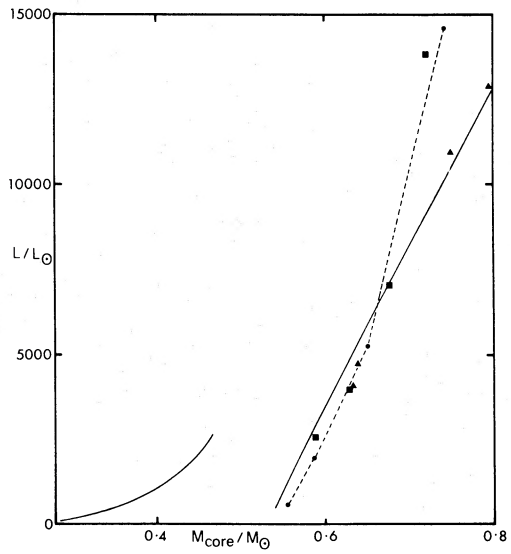

FIG. 1.—The cores of the four models in the $(L/L_\odot, M_{core}/M_\odot)$-plane (*squares*). A first-giant-branch track of Rood (1972) and the track given in fig. 3 of Paczyński (1970) are shown as solid lines. Cores of double-shell-source models in the evolutionary sequences of Rose and Smith (1970) (*triangles*) and Sweigart (1971) (*circles* and *dotted line*) are also shown.

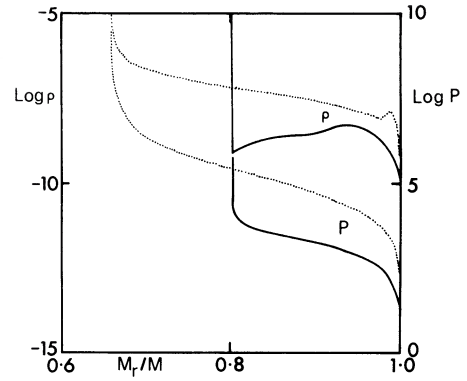

FIG. 2.—Log P and log ρ plotted against mass fraction for model 1 (*dotted line*) and model 4 (*continuous line*).

The temperature distribution within the envelope of models 1 and 4 is shown in figure 4. A maximum in the temperature gradient occurs just outside the convection zone where the opacity of the H^- ion dominates. Interior to this region, the onset of efficient convection reduces the temperature gradient while a decrease in the opacity at larger radii produces a smaller temperature gradient there. Figure 4 also shows the fraction of the flux carried by convection throughout the envelope in the two models. It is clear that the onset of convection is very rapid at the outer edge of the convection zone and that the outer edge moves inward in mass as the luminosity increases. Since the strongest driving of the envelope occurs at the outer edge of the convection zone (see Keeley 1970*b* and § III), the fraction of the mass of the envelope above the convection zone is a critical factor in determining whether the envelope will pulsate in the fundamental or an overtone mode.

The total energy E (internal + gravitational) of all matter above a given radius in model 4 is plotted against the radius in figure 5. Neutral atoms of

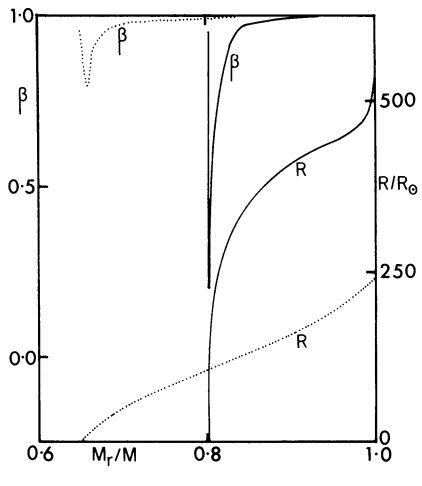

FIG. 3.—Radius and $\beta = P_{gas}/P$ plotted against mass fraction for model 1 (*dotted line*) and model 4 (*continuous line*).

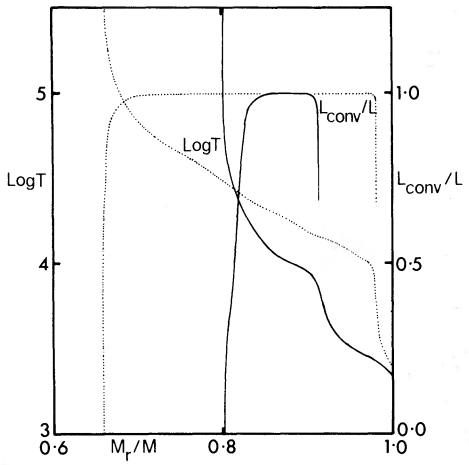

FIG. 4.—Log T and the fraction of the energy flux carried by convection plotted against mass fraction for model 1 (*dotted lines*) and model 4 (*continuous lines*).

hydrogen and helium at 0° K are assumed to have zero internal energy. Although the energy per unit mass of the outermost (partly molecular) material is negative, the ionization energy of hydrogen and helium, together with the energy of radiation trapped within the envelope, is sufficient to make E positive throughout much of the envelope. Hoyle (1956) and Paczyński and Ziołkowski (1968) pointed out this feature of very luminous red-giant envelopes and suggested that an efficient conversion of the envelope energy to kinetic energy could cause mass loss with velocities at infinity of a few tens of kilometers per second. However, the detailed dynamical calculations of Keeley (1970*b*), Smith and Rose (1972), and this paper show that the behavior of red-giant envelopes is highly nonadiabatic; direct conversion of the internal energy of the envelope to kinetic energy does not therefore occur.

b) Evolution in the H-R Diagram

Figure 6 shows the position of the four models in the ($\log L/L_\odot$, $\log T_e$)-plane. A first-giant-branch (FGB) evolutionary track of Rood (1972) is shown for comparison. Since tracks of FGB stars of other recent

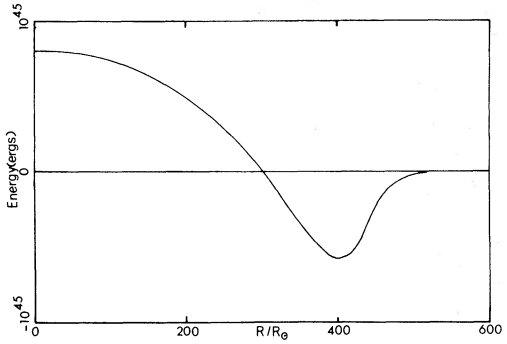

FIG. 5.—The total energy of all matter above a given radius plotted against radius in model 4.

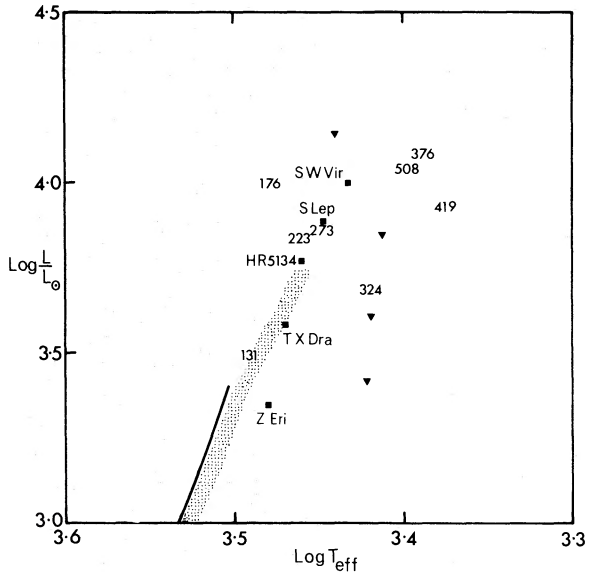

FIG. 6.—Position of the four models in the ($\log L/L_\odot$, $\log T_e$)-plane (*filled triangles*). The solid line is the first-giant-branch evolutionary track of Rood (1972), while the numbers (periods in days) mark the positions of the groups of long-period variables discussed by Osvalds and Risley (1961). The shaded region is a calibration of the old-disk giant branch by Eggen (1973) (see text for further details).

authors (Eggleton 1968; Iben 1968; Demarque and Mengel 1973; Faulkner and Cannon 1973) all terminate at $\log L/L_\odot \lesssim 3.4$, the four models considered here are more luminous than stars on the FGB.

The dotted region in figure 6 is a calibration of the observed giant branch by Eggen (1973), based on the old-disk groups ζ Herculis, 61 Cygni, and Wolfe 630. The filled squares represent some variables on the giant branch of these groups given by Eggen (1971*c*). Table 5 of Eggen (1971*b*) is used to obtain $\log T_{eff}$ from the $(R - I)_K$ colors. The numbers on figure 6 are the mean periods in days of the groups of long-period variables studied by Osvalds and Risley (1961). Smak's (1964, 1966) calibrations of effective temperature and luminosity are used to place the groups in the ($\log L/L_\odot$, $\log T_e$)-plane. The data refer to maximum light, but for reasonable (1 mag) variations in bolometric luminosity (Pettit and Nicholson 1933), all groups except those of period 131 days and 324 days lie well above the theoretical FGB at mean luminosity. Many long-period variables must therefore be AGB stars. As seen from figure 6, the four models described in this paper lie in the region of the H-R diagram occupied by the long-period variables.

It is interesting to compare the expected number of FGB and AGB stars at a given luminosity. Assuming that the mass function is constant over the small range of initial stellar masses present on the AGB, the number n of stars per unit interval in $\log L/L_\odot$ on either giant branch obeys the relation

$$\frac{1}{n} \propto \frac{d \log L/L_\odot}{dt} = \frac{d \log L/L_\odot}{dM_{\rm core}} \frac{dM_{\rm core}}{dt} ,$$

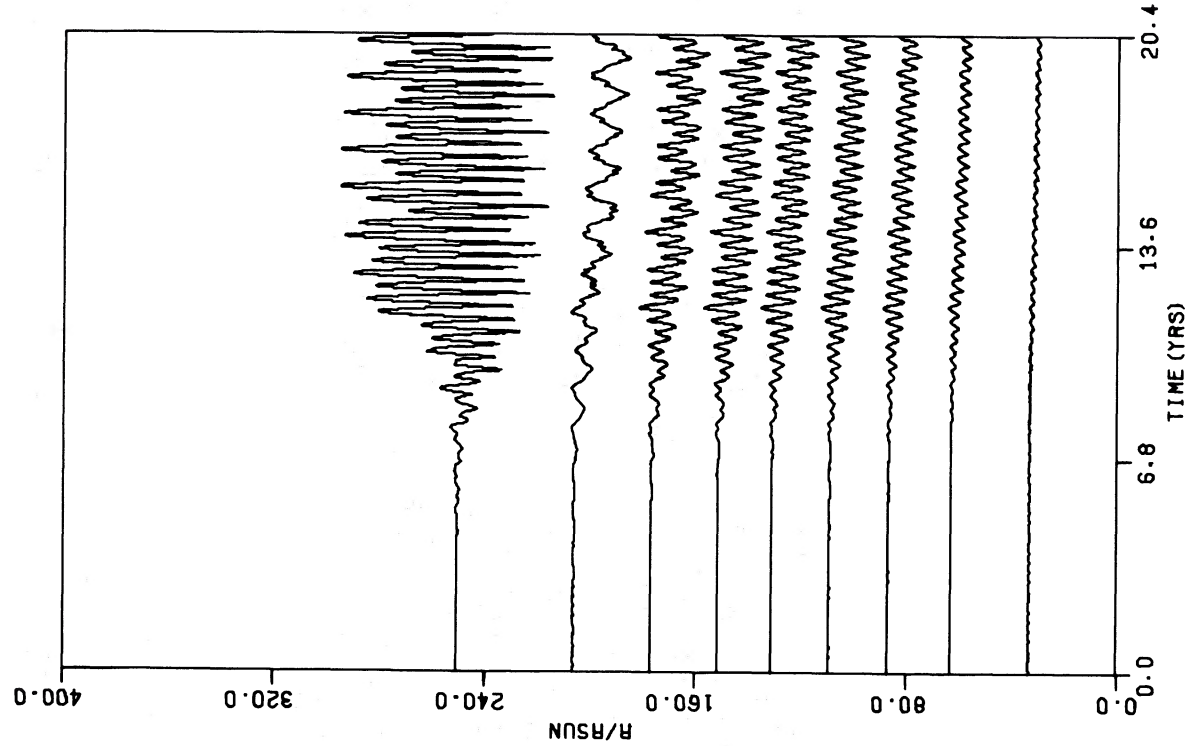

FIG. 8

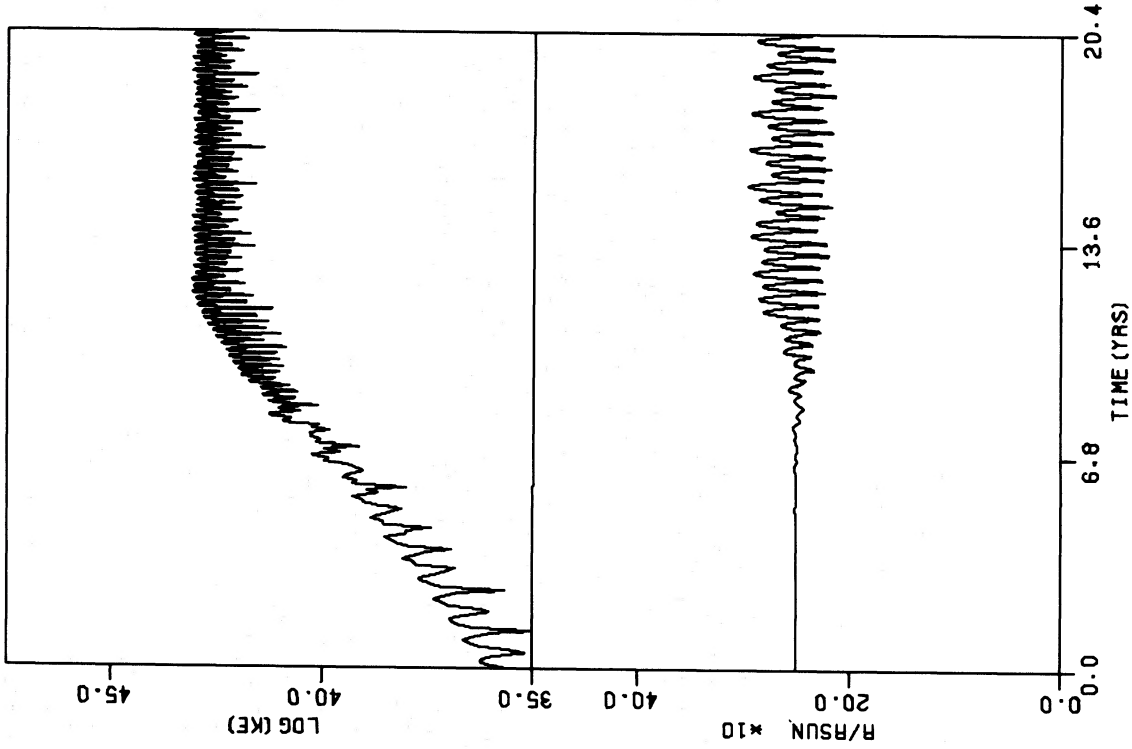

FIG. 7

FIG. 7.—Envelope kinetic energy (ergs) and surface radius as a function of time in model 1.
FIG. 8.—Radius variation with time in model 1 for points at mass fractions 0.9995, 0.9605, 0.9216, 0.8792, 0.8411, 0.7989, 0.7599, 0.7215, and 0.6810.

where $M_{\rm core}$ increases monotonically with $L/L_\odot$. With a constant mass fraction of hydrogen in the envelope,

$$dM_{\rm core}/dt \propto L/L_\odot ,$$

since on the first giant branch all the luminosity comes from the hydrogen-burning shell while on the AGB most of the luminosity is produced by the hydrogen-burning shell and the mass fraction separating the two burning shells does not vary rapidly with $M_{\rm core}$. Combining the above results gives

$$\frac{1}{n} \propto \frac{dL/L_\odot}{dM_{\rm core}} .$$

From figure 1 it can be seen that the slope of the (luminosity, core mass)-relation on the FGB increases with luminosity while on the AGB the slope is roughly constant for $L \leqslant 8000\ L_\odot$. At $\log L/L_\odot = 3.4$ there are roughly equal numbers of AGB and FGB stars. Since the (luminosity, core mass)-relations are reasonably independent of input parameters (total mass, Z) and uncertainties in the physics of envelope convection, the relative number densities of FGB and AGB stars should be a function of luminosity alone.

III. DYNAMICAL BEHAVIOR OF MODEL 1

a) Results of the Numerical Calculations

Figure 7 shows the growth of the envelope kinetic energy from a homologous perturbation with a surface velocity of 100 cm s^{-1}. Initially, the envelope pulsates in the fundamental mode due to the form of the initial perturbation and because the time-step (0.05 years) used in the early phases is too long to allow the development of the first overtone. At low amplitudes, the oscillations grow exponentially with an e-folding time of 1.49 years and a period of 482 days. With the reduction in the size of the time-step, a strong first-overtone mode develops and continues to grow in amplitude until the rapid onset of equilibrium when the peak kinetic energy of the envelope has reached $10^{42.4}$ ergs. At full amplitude, a fundamental component is still present in the pulsation as clearly seen in figure 8. The node of the first overtone is situated near the middle of the hydrogen ionization zone at mass fraction $q = 0.96$ (see fig. 11).

A notable feature of the behavior of this model is the slow contraction evident in figure 8. This is consistent with the fact that the average radiated luminosity is greater than the luminosity at the base of the envelope. Keeley (1970*b*) also found that pulsation of a static model caused it to contract. In the present study, no large change in the period of the model resulted from structural rearrangement over the time interval studied and the peak kinetic energy remained constant throughout the contraction phase. On the other hand, Keeley (1970*c*) found that the period of his model decreased from 520 days to 300 days in 37 cycles. Differences in the physics of convection and in

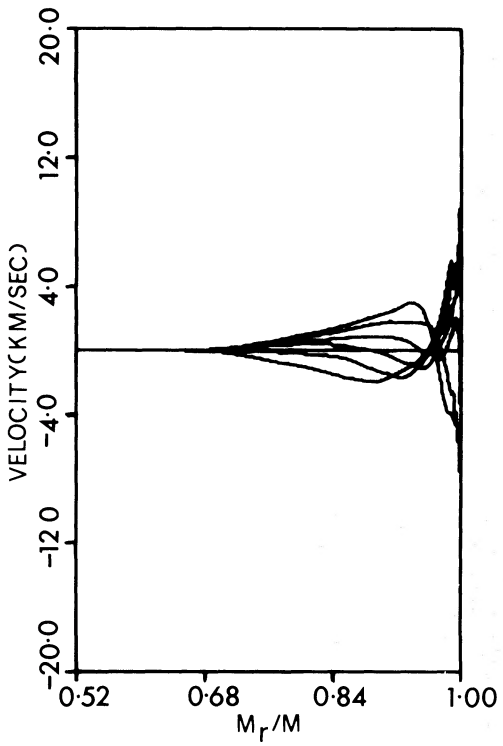

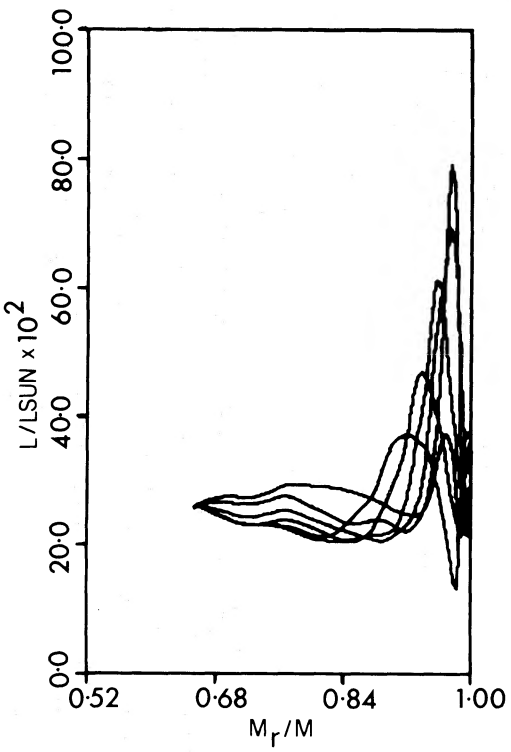

FIG. 9*a* (*left*).—Velocity (positive velocity is away from stellar center) as a function of mass fraction in model 1 at 0.03-year time intervals over one-half cycle. The surface velocity is increasing with time.

FIG. 9*b* (*right*).—Luminosity profiles corresponding with the velocity profiles in fig. 9*a*. The interior luminosity peak decreases with time.

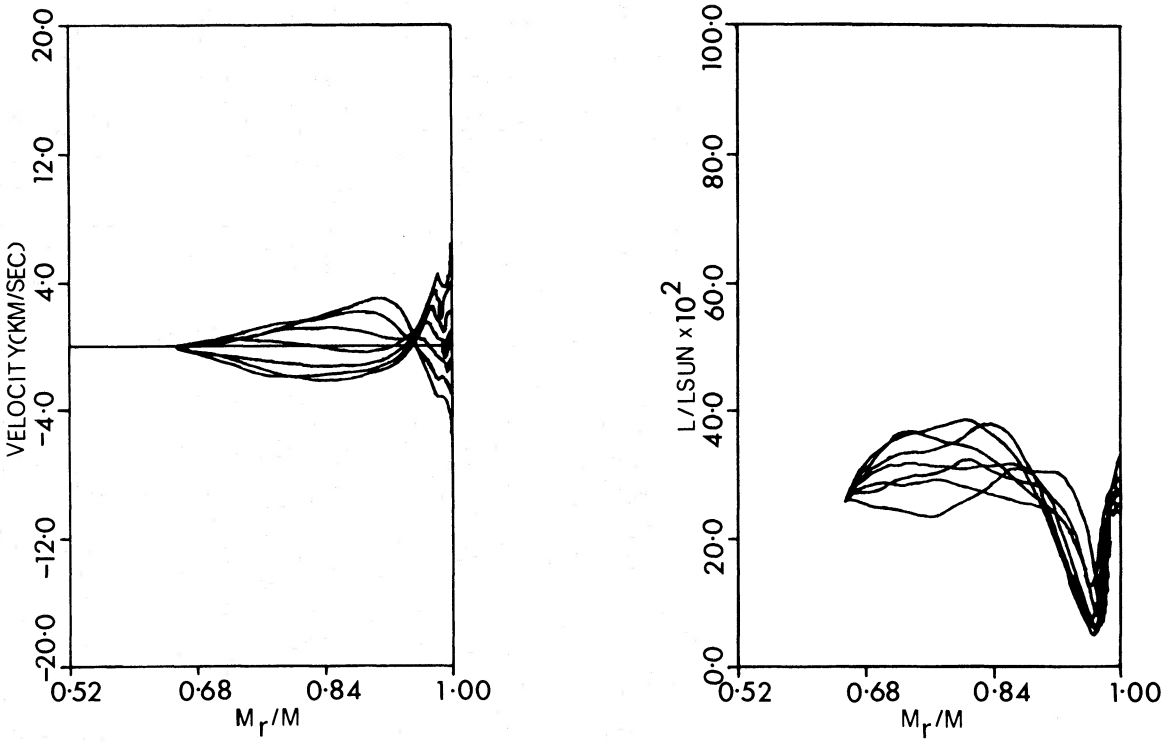

FIG. 10*a* (*left*).—Velocity as a function of mass fraction in model 1 at 0.03-year time intervals over the half-cycle immediately following that shown in fig. 9*a*. The surface velocity is decreasing with time.

FIG. 10*b* (*right*).—Luminosity profiles corresponding with the velocity profiles in fig. 10*a*.

the pulsation amplitude probably account for the small contraction of model 1 compared with Keeley's fundamental pulsator.

Figures 9*a* and 10*a* show the velocity as a function of mass fraction within the envelope over two successive half-cycles. The velocity gradient at the surface is very steep, and the velocity amplitude at the surface is much larger than the velocity amplitude interior to the node. Within the convection zone the velocity profile is smooth, but the exterior layers tend to decouple from the motion of the interior. A shock front separates the two regions when the matter in

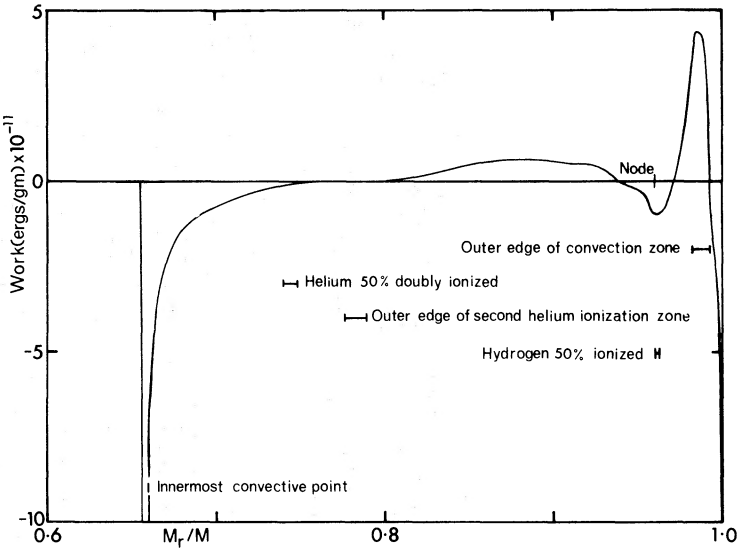

FIG. 11.—Work per gram done in model 1 over three successive first overtone cycles. Movement of some specified features within the envelope is shown schematically.

the convection zone begins to move outward into the infalling surface material. It is the emergence of the shock front at the surface that gives rise to the sawtooth nature of the surface velocity curve (see fig. 12).

Interior luminosity profiles are shown in figures 9*b* and 10*b*. The variation in surface luminosity is much less than the interior luminosity variation as most of the absorption and release of energy occur in the hydrogen and He I ionization zones. A large contribution to the surface luminosity comes from the strong shock front near the surface in the time interval immediately preceding velocity reversal at the surface.

Figure 11 shows the work done within the envelope over three successive first-overtone cycles (this also corresponds with approximately one fundamental cycle). The overall work done is nonzero due to the superposed fundamental mode. Two strong dissipation regions exist, one at the surface and one at the base of the envelope. The dissipation at the surface is caused by shock waves.

The strongest driving is produced by matter in the outer parts of the convection-ionization zone, particularly by that matter which passes in and out of the zone. Keeley (1970*b*) also found driving in this region and pointed out that uncertainties in the molecular opacity were therefore unlikely to directly affect the driving of theoretical models. A second driving region appears to exist in the hydrogen–He I ionization region interior to the node.

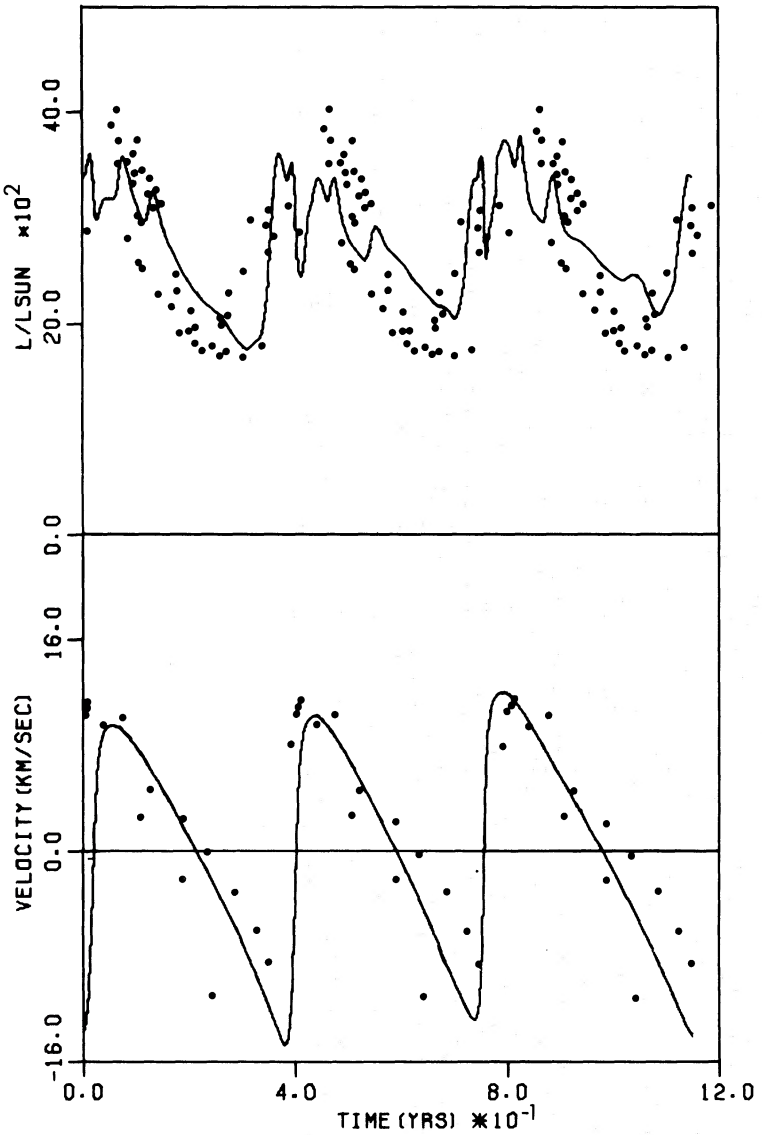

FIG. 12.—Surface velocity and luminosity as a function of time over three first overtone periods in model 1. *Circles*, the observed velocity and luminosity of S Car (see text).

b) *Comparison with Observation*

Model 1 is compared directly with the high-velocity halo variable S Carinae whose period (150 days) is close to that of the model (146 days). It should be noted that the observational estimate of the effective temperature of S Car is $\sim 600°$ K hotter than the effective temperature of the model. The combined observational and theoretical errors in $T_{\rm eff}$ are unlikely to amount to 600° K. Also, the metal abundance in S Car (Hain 1969) is approximately 0.1 times the solar metal abundance which is used in model 1. In view of these factors and the large uncertainties in the physics of convection, only qualitative agreement between theory and observation is expected.

The surface velocity and luminosity are plotted in their correct relative phase for three cycles in figure 12. The velocity points are the observed infrared absorption line velocities of Hain (1969). A mean radial velocity of 287.7 km s^{-1} has been assumed. Phase 0.0 corresponds to the velocity maximum at $t \sim 0.4$ years, and the observational data are repeated over three cycles with a period of 146 days (the computed overtone periods vary slightly throughout a fundamental cycle and average 146 days).

The luminosity is derived from the data of Eggen (1972*a*, private communication). All observations are reduced to a 150-day cycle, assuming a phase of 0.5 at the visual light minimum on JD = 2,440,680. (Hain 1969 also took phase 0.5 to correspond with the visual light minima.) Using the transformations of Eggen (1971*a*), the I_J magnitude is derived from the photometric (R, I) magnitudes on the Kron system. The apparent bolometric magnitude is then obtained from the relation $M_{\rm bol} = M(I_J) + 1$ given by Eggen (1971*b*) and verified for Population II stars by Glass and Feast (1973). If one assumes a distance modulus of 8.15 for S Car, the average luminosity of model 1 agrees with the average luminosity of S Car.

It can be seen that the shape and magnitude of the computed velocity curve agree well with the observations. The amplitude of the luminosity curve and its phase relative to the velocity curve are also in reasonable agreement with the observations. A notable feature of the theoretical luminosity curve is the consistent appearance of three main peaks. The first peak is produced by the shock front near the surface. When all the surface layers have passed through the shock front (coinciding with the velocity reversal at the surface), the luminosity drops to a secondary minimum. The existing red and infrared observations are not sufficiently detailed to show such a minimum, if it really occurs. However, the photoelectric V light curve of Wisse and Wisse (1971) does show a leveling off on the rising branch which may correspond with a bolometric luminosity minimum. The hump on the declining edge of the theoretical light curve originates in the outer parts of the hydrogen ionization zone and is caused by a relatively rapid inward movement of the ionization zone.

The results of Hain (1969) show that the amplitude of the velocity curve obtained from the red spectra of S Car is considerably smaller than that obtained from the infrared spectra. Hain pointed out that the red velocity curve arises from deeper within the star than the infrared velocity curve since the opacity at 8000 Å is higher than the opacity at 6000 Å. The difference in the amplitudes of the red and infrared velocity curves can be explained by the very steep velocity gradient at the surface shown in figures 9*a* and 10*a*.

Strong Hα emission in the spectrum of S Car has been noted by Hain (1969), the emission being faintly visible at phase 0.6, very strong at phase 0.0, and disappearing at phase ~ 0.25. The observed emission probably originates in the shock front which first forms in the model at phase ~ 0.65. The shock emerges at the surface at phase 0.0 when the observed emission is strongest. In the model, the shock disappears at this point; but in a real giant star where the density does not suddenly drop to zero as in a theoretical model, the shock could continue to travel outward and maintain the emission for some time.

It is interesting to compare the overall contraction found here and by Keeley (1970*c*) with observation. The results of Eggen (1971*c*, 1972*b*) show that large amplitude red variables lie on the cool side of the $(M_{\rm bol}, R - I)$-relation defined by small-amplitude variables. This suggests that pulsation may cause an expansion rather than a contraction of the average radius, in contrast to the theoretical results.

IV. DYNAMICAL BEHAVIOR OF MODEL 2

a) *Results of the Numerical Calculations*

Figure 13 shows the growth of the kinetic energy of model 2. As with model 1, the envelope begins pulsating in the fundamental mode but soon develops a strong first overtone. However, in contrast to model 1, the fundamental mode continues to grow, and it eventually overwhelms the first-overtone pulsation.

Following the radius minimum at $t = 13.6$ years in figure 14, the envelope undergoes a large expansion which is associated with a large inward movement (in mass) of the ionization and convection zones. A shock front forms at the outer edge of the hydrogen ionization zone (see fig. 15*a*), matter being accelerated out to the shock front and into the overlying shell of neutral material. In the early stages of the expansion most of the luminosity is produced by the release of ionization energy of hydrogen at the shock front, as seen in figure 15*b*. Later in the expansion, the outer shell and the expanding material interior to it maintain their identity, although the velocity discontinuity separating these two regions is gradually smeared out. The outer edge of the convection zone moves in to a minimum mass fraction 0.892 during the expansion.

Since much of the internal energy of the envelope was radiated away during the expansion, the envelope now has insufficient pressure to support itself and it undergoes a large collapse (see fig. 14). During the ensuing rebound, 3.1 percent of the mass of the star (19 zones) reaches escape velocity. Figure 16 shows that effectively all the kinetic energy of the rebound is

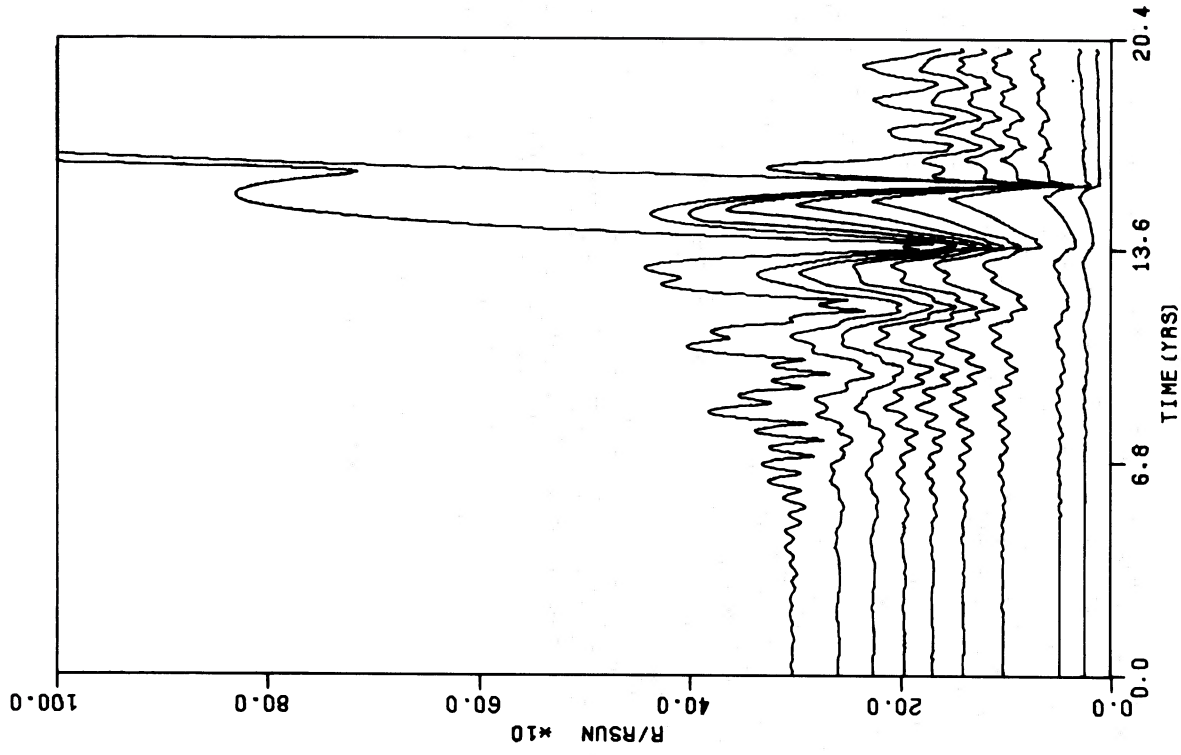

FIG. 14

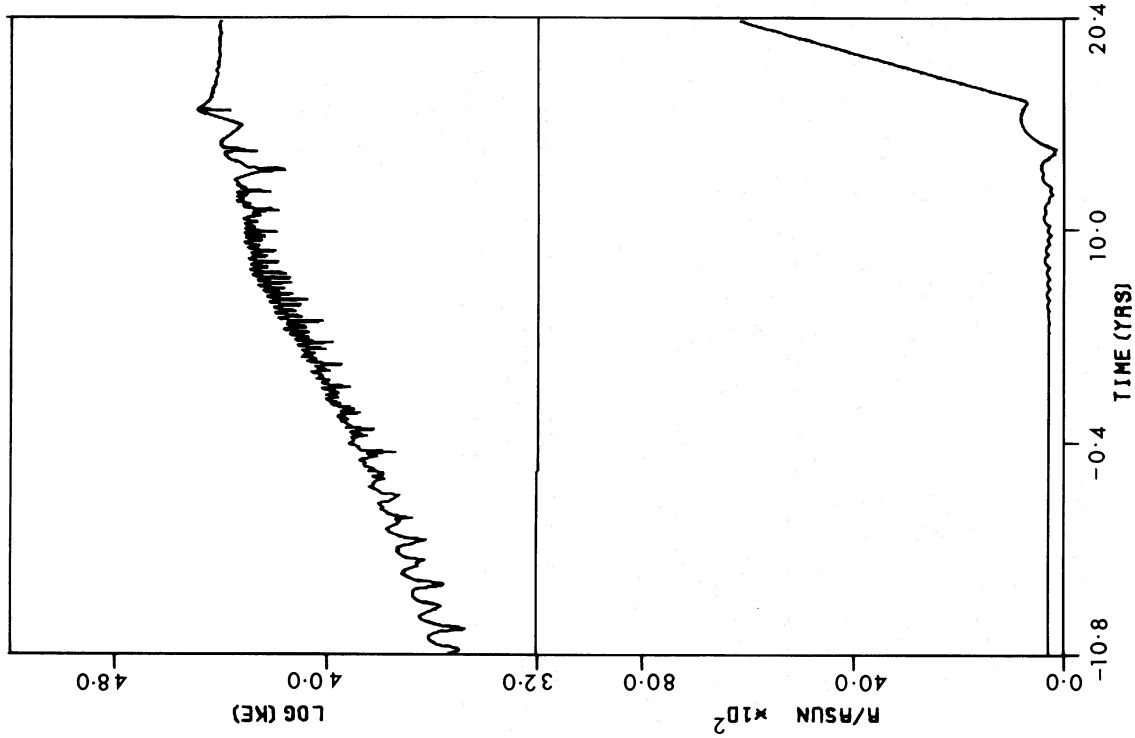

FIG. 13

FIG. 13.—Envelope kinetic energy and surface radius as a function of time in model 2.

FIG. 14.—Radius variation with time in model 2 for points at mass fractions 0.9995, 0.9609, 0.9205, 0.8800, 0.8412, 0.8015, 0.7608, 0.7201, and 0.7103.

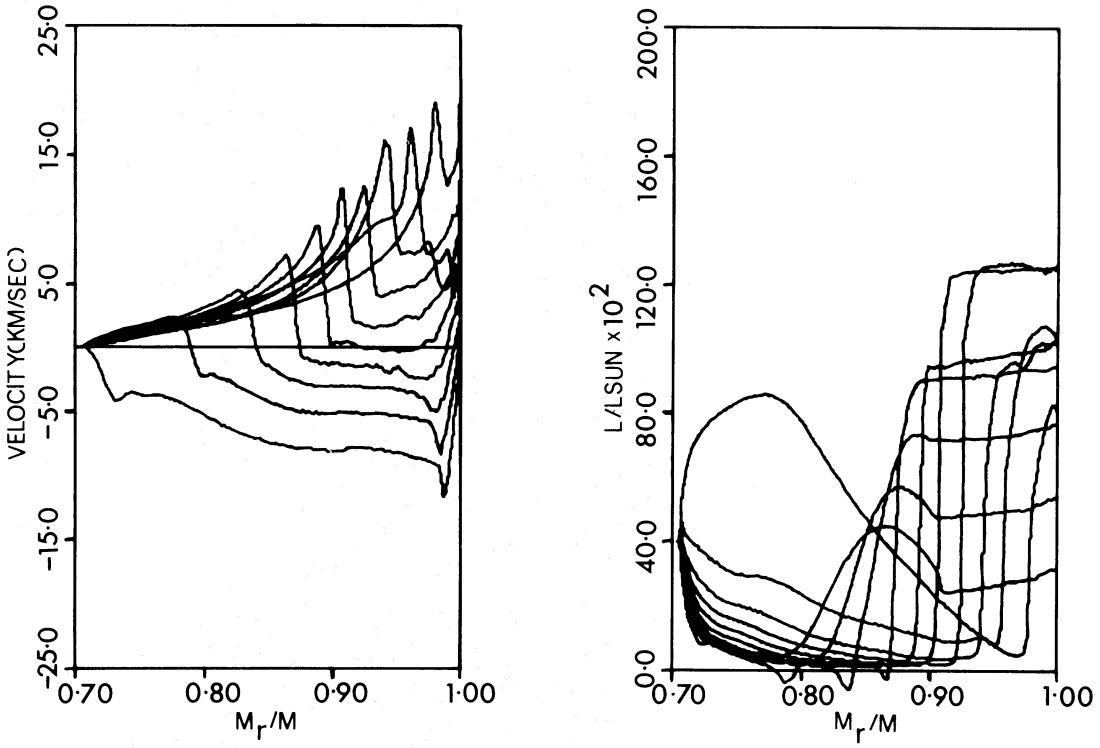

FIG. 15*a* (*left*).—Velocity as a function of mass fraction in model 2 at 0.15-year time intervals during the expansion and early collapse phases. The shock front moves inward in mass fraction with time.

FIG. 15*b* (*right*).—Luminosity profiles corresponding with the velocity profiles in fig. 15*a*. Most of the luminosity is produced by the liberation of the ionization energy of hydrogen during the expansion.

imparted to the envelope during a very small time interval corresponding to maximum compression.

After ejection of the surface layers, the remaining envelope begins to pulsate once again. The period and the average radius of each point increase with time since the energy radiated by the envelope is less than the energy input from the core. Meanwhile, matter that has been removed from the star (but which has not reached escape velocity) continues to fall back onto the star in a shock front (see fig. 17). The hydrogen in the envelope above the shock front is completely molecular and has a temperature of $\sim 500°$ K. This temperature is only a rough estimate since the diffusion equation is used to describe energy transfer and the radius and temperature differences between points in the remnant star and points in the ejected envelope are very large. Another major uncertainty in the models at this stage is the value of the water molecule opacity, which is treated only approximately by the formula of Paczyński (1969). The opacity of the material in the ejected envelope is produced entirely by water molecules.

The above results indicate that as soon as the luminosity of a 0.9 $M_\odot$ star becomes sufficient to cause pulsation in the fundamental mode ($\log L/L_\odot \approx 3.6$), severe mass loss will occur. On the AGB, the necessary luminosity will be first produced during a thermal instability of the helium-burning shell.

b) Comparison with Observations

There is convincing observational evidence for mass loss from red variable stars. The violet-shifted absorption lines exhibited by some Mira variables (Merrill 1960) indicate the presence of an outward-moving circumstellar shell of gas. Thirteen late-type stars with infrared excesses examined by Hyland, Becklin, and Neugebauer (1972) are Mira variables with periods from 300 days to 800 days. The infrared excess is produced in a circumstellar dust shell which Hyland *et al.* estimate to have a typical mass $\sim 2 \times 10^{27}$ g. Radio emission from these objects at 1612 MHz indicates that a gas shell containing OH molecules coexists with the dust shell. Ejection of matter by pulsation during the luminosity increase associated with an earlier shell thermal instability could account for the gas and dust surrounding some Mira variables.

Iben and Rood (1970) and Demarque and Mengel (1972) have noted that variable mass loss amounting to $\sim 0.2\ M_\odot$ is required on the first giant branch to explain the masses of horizontal-branch stars. The luminosity $\log L/L_\odot \leqslant 3.4$ at the tip of the first giant

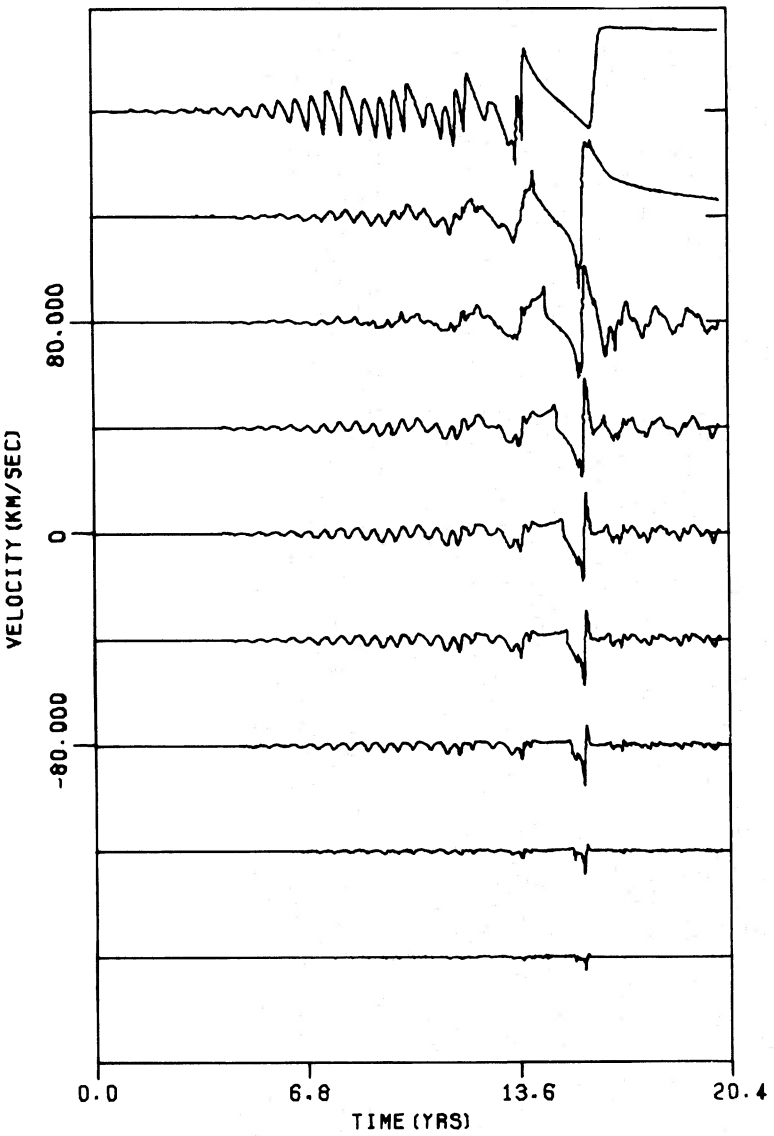

FIG. 16.—Velocity variation with time in model 2 for points at the mass fractions specified in fig. 14

branch (Eggleton 1968; Iben 1968; Rood 1972; Demarque and Mengel 1973; Faulkner and Cannon 1973) is only slightly less than that at which large-scale mass loss was found in this study for a 0.9 $M_\odot$ star. Since the luminosity required to produce pulsational mass loss is sensitive to variations in the treatment of convection (see § VII) and to envelope mass (see § VIII), it is possible that pulsational mass loss at the tip of the first giant branch could explain the $\sim 0.2\ M_\odot$ mass difference between horizontal branch stars and stars at the main-sequence turnoff of globular clusters.

Another form of mass loss which probably occurs from red-giant stars is planetary-nebula ejection (Abell and Goldreich 1966). However, the nucleus of a planetary nebula must have $\lesssim 2 \times 10^{-3}\ M_\odot$ of hydrogen-rich material left on its surface at ejection if it is to evolve on a time scale of $\sim 2 \times 10^4$ years (Osterbrock 1964) and attain the high effective temperatures found on the Harman-Seaton sequence. Unless all but a very small fraction of the envelope can be removed by repeated ejections over a period much less than 10^4 years, it is difficult to associate planetary-nebula ejection with the mass loss found in this model.

V. DYNAMICAL BEHAVIOR OF MODEL 3

a) Results of the Numerical Calculations

The plot of envelope kinetic energy against time in figure 18 shows the growth of the small-amplitude

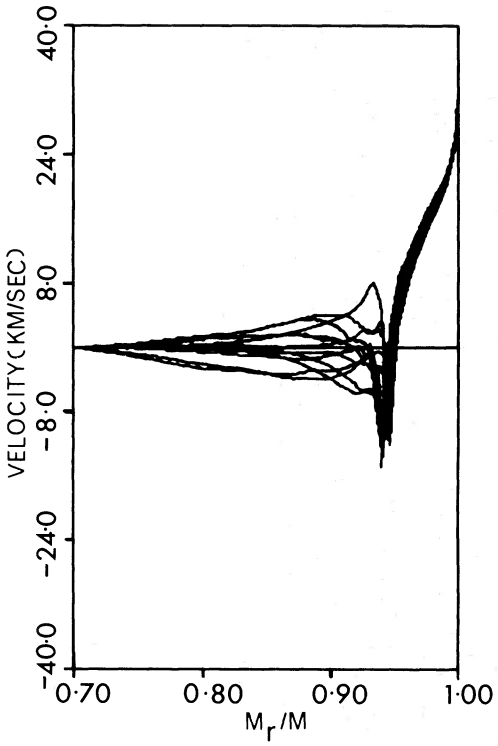

FIG. 17.—Velocity as a function of mass fraction in model 2 at 0.15-year time intervals following the ejection of the surface layers. The interior of the envelope is pulsating while the decoupled shell of ejected matter can be seen above the shock front at the surface of the pulsating region.

linear pulsation and the rapid transition to nonlinear behavior. Figures 19*a* and 19*b* show velocity and luminosity profiles within the envelope during small-amplitude pulsation. A noticeable feature of the profiles is the large amplitude deep within the envelope. This type of profile, which was also found in model 4 but not in models 1 and 2, is probably the result of the shell-like structure of static high-luminosity envelopes. As a result of the large amplitude (and damping, as shown in fig. 11), deep within the envelope care must be taken to apply the inner boundary conditions close to the core.

Immediately preceding the first collapse seen in figure 20 the envelope undergoes a large expansion which coincides with the transition to highly nonlinear behavior. The expansion is accompanied by a recession from the surface (in mass) of the convection-ionization zone, with most of the ionization energy of the envelope being radiated away through the regions of low opacity above the ionization zone. Following the expansion, the envelope has insufficient internal energy remaining to support itself and it collapses. After some rebounding, the envelope settles into a compact state and begins pulsating. The input luminosity to the envelope now exceeds the radiated luminosity (fig. 21), and the envelope begins to expand, with an increase in period resulting. Finally, when the internal energy has built up sufficiently, the envelope undergoes another expansion and subsequent collapse.

Figures 22*a* and 22*b* show velocity and luminosity profiles during the second expansion. Most of the luminosity is produced by release of the ionization energy of hydrogen over a region of very small mass. Matter is accelerated outward to the shock front at the ionization zone where it collides with a shell of denser neutral material moving outward at ~ 3 km s^{-1}. The motion of this shell, which can be recognized in figure 20 as the set of parallel lines near the tip of the expansion, is partly sustained by the momentum of material colliding with its base (for most of the expansion, the pressure is 2–3 times as large within the base of the envelope as below it). Eventually, the convection zone disappears completely and the hydrogen ionization zone ceases to move inward in mass, resulting in a large drop in luminosity and the second collapse of the envelope. At the peak of the expansion, the mass fraction between the hydrogen-burning shell and the hydrogen ionization zone is only 0.002. The second expansion and collapse should be typical of that in subsequent relaxation cycles since the initial static structure will have no effect on the structure of the envelope after the first violent collapse. In summary, the full amplitude dynamical behavior of this model is characterized by relaxation oscillations with a period ~ 7 years. Smith and Rose (1972) have reported similar relaxation oscillations in a 0.856 $M_\odot$ red-giant star.

b) Comparison with Observations

This model may explain the behavior of a subclass of the symbiotic stars. The light curves of the symbiotic

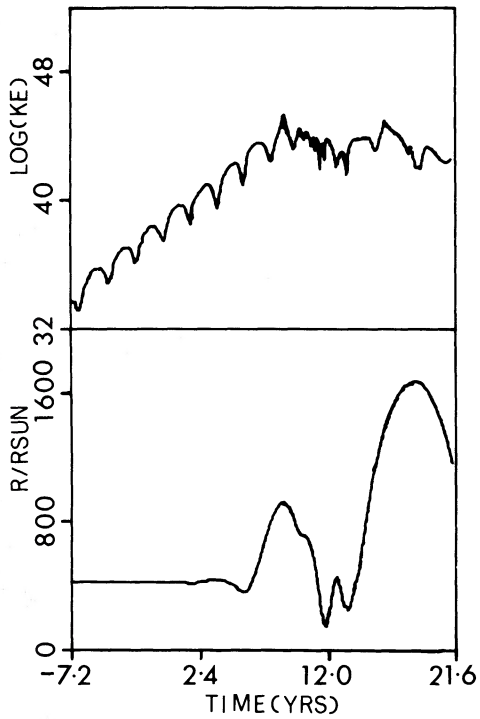

FIG. 18.—Envelope kinetic energy and surface radius as a function of time in model 3.

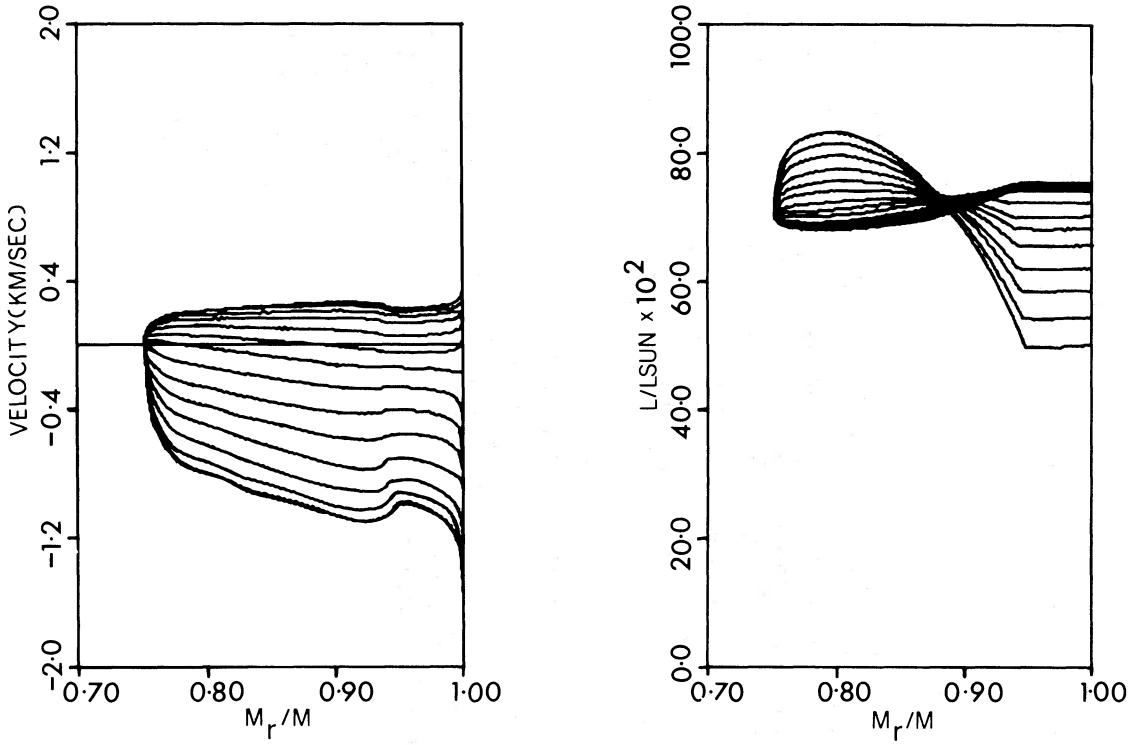

FIG. 19*a* (*left*).—Velocity as a function of mass fraction in model 3 at 0.15-year time intervals during small-amplitude pulsation. The surface velocity is decreasing with time.

FIG. 19*b* (*right*).—Luminosity profiles corresponding with the velocity profiles in fig. 19*a*. The surface luminosity is decreasing with time.

stars vary with a semiregular period typically 200–800 days while larger eruptions occur on a time scale of ~3.5 years (Payne-Gaposhkin 1964). Sahade (1960) describes the spectrum of a symbiotic star as follows: "(*a*) When the star is faint, an M-type absorption spectrum is prominent; (*b*) when the star brightens, a B-type shell spectrum develops, its continuum dominating the photographic region and covering the M-type spectrum; and (*c*) when the star declines in brightness, the shell spectrum weakens, and emission lines of progressively increasing excitation and forbidden transitions develop."

Some suggestions which have been advanced to explain the combination spectrum and eruptive behavior of the symbiotic stars are: (*a*) the symbiotic stars are binaries consisting of a hot and a cool component (Hogg 1934; Berman 1932); (*b*) the symbiotic stars consist of a single hot star surrounded by a large optically thick envelope giving the appearance of a hot continuum with the absorption spectrum of a cool star superposed on it (Sobolev 1960); (*c*) the symbiotic stars are single cool stars surrounded by a shock-wave–heated chromosphere (Aller 1954; Gauzit 1955).

Although some of the symbiotic stars are undoubtedly binaries (for example, AR Pav, T CrB), the behavior of model 3 may explain others in conjunction with hypothesis (*c*) above. The underlying periodicity and eruptive behavior are explained directly by model 3. In order to explain the chromosphere, it should be remembered that the large expansion and accompanying high luminosity (an eruption) are associated with a strong shock front in the envelope. Noise from this shock could propagate outward through the overlying shell of neutral material and dissipate in the outer regions of the star to produce the chromosphere. The irregularities in the density caused by the convection in the material incident at the shock front will enhance noise production. An upper limit to the rate of production of sound energy can be obtained from an analysis similar to that by Schwarzschild (1948) for the solar chromosphere. The upper limit is $L_{\text{sound}} = 4\pi r^2 \rho \omega^2 V$, where ω is the material velocity (set equal to the velocity difference across the shock front for an upper limit), V is the sound velocity, ρ is the density, and r is the radius of the shock front. At mid-expansion, the production of sound energy given by the above formula is $\sim 2700\, L_\odot$. Even after allowing for the overestimates in this formula, it seems that a significant flux of sound energy is available during the expansion to energize a blue continuum. The blue continuum could be produced by two-photon emission, H^- ion formation, and recombination in a collisionally excited hydrogen-rich plasma (Gerola and Panagia 1968, 1970).

An estimate of the time for sound to cross the shell in the early phases is ~0.5 years (assuming typical values $\log P = 2.4$, $\log \rho = -9$, shell width $= 100\, R_\odot$).

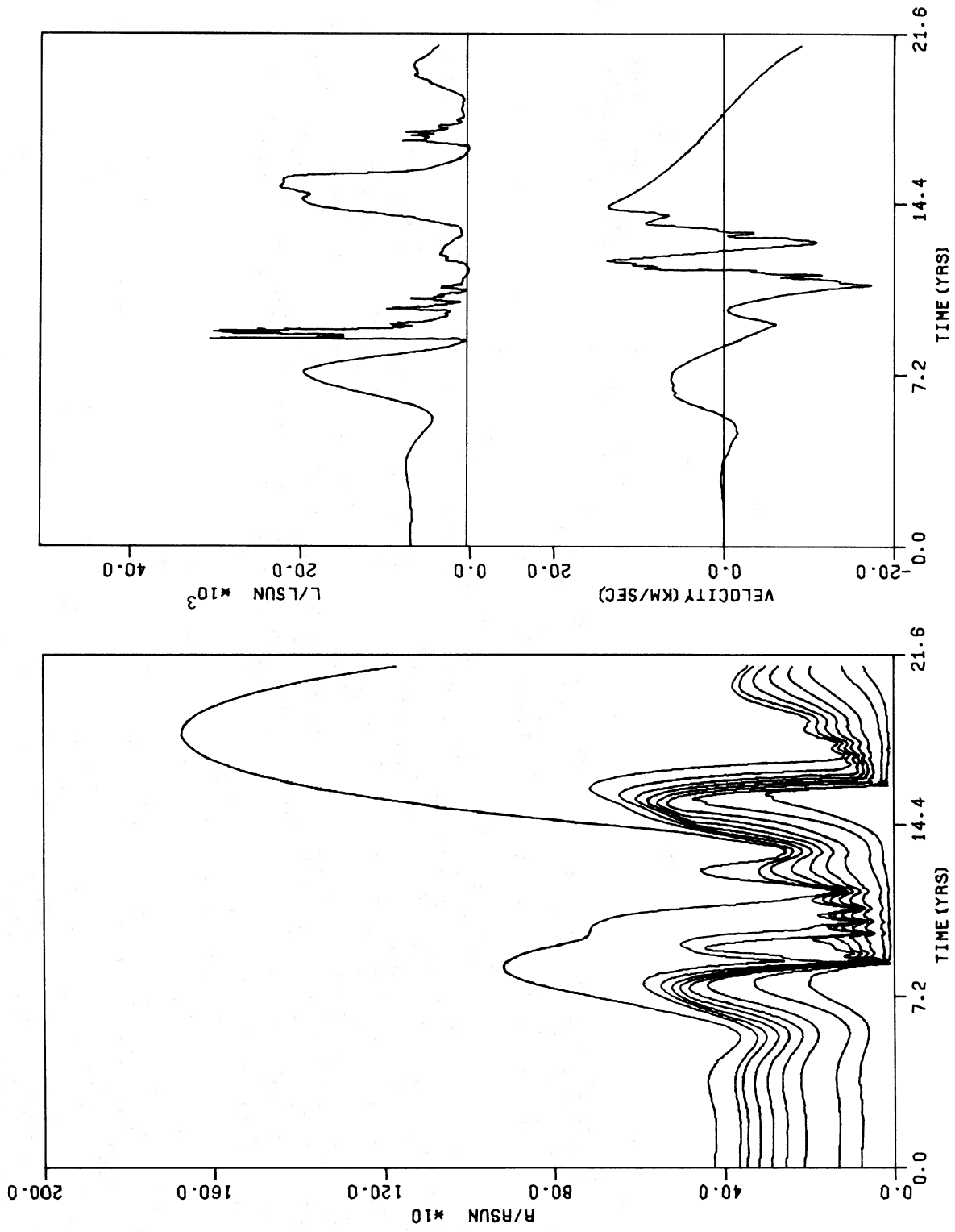

FIG. 20

FIG. 21

FIG. 20.—Radius variation with time in model 3 for points at mass fractions 0.9995, 0.9657, 0.9327, 0.8996, 0.8666, 0.8334, 0.8001, 0.7653, and 0.7556.
FIG. 21.—Surface velocity and luminosity in model 3 as a function of time.

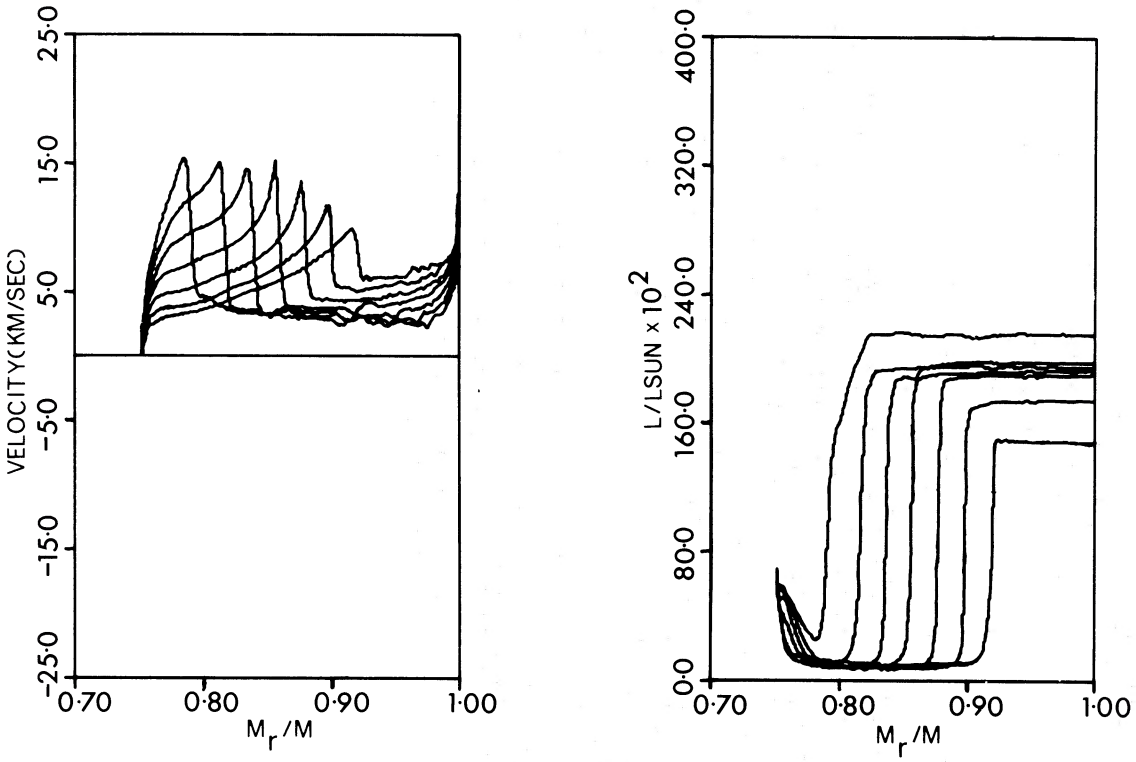

FIG. 22*a* (*left*).—Velocity as a function of mass fraction in model 3 at 0.15-year time intervals during the second expansion. The outward-moving shell of neutral material and the shock front at its base are clearly seen. The shock front moves inward in mass fraction with time.

FIG. 22*b* (*right*).—Luminosity profiles corresponding with the velocity profiles in fig. 22*a*.

Faraggiana and Hack (1971) found that it took about 1 year from the beginning of the flare-up of CH Cyg for a chromosphere to form. As the shock front moves inward in mass and the envelope expands, the time for sound to cross the outer shell will increase, causing a prolonging of the excitation mechanism. Dissipation at later times high in the residual low-density envelope above the star could provide the energy necessary to produce the high-excitation and forbidden emission lines. It should be noted that the shock front associated with the envelope collapse will not cause any noise dissipation in the envelope, as the infall velocity must exceed the sound velocity at the shock front.

VI. DYNAMICAL BEHAVIOR OF MODEL 4

a) Results of the Numerical Calculations

The dynamical behavior of this model is an extreme example of the relaxation oscillations shown by model 3 and is accompanied by mass loss from the envelope. Figure 23 shows the kinetic energy and the surface radius as a function of time. The expansion-collapse-rebound phase is illustrated in figure 24 while some velocity and luminosity profiles during this phase are shown in figures 25*a* and 25*b*. Reversal of the collapse coincides with the extremely large flux of luminosity in the interior [peak $\log (L/L_\odot) = 5.16$] seen in figure 25*b*.

Figure 26 shows some velocity profiles during the rebound. Matter is accelerated outward to the ionization zone which coincides with (or is slightly interior to, at later stages) a shock front at the base of a compact shell of neutral material moving outward at ~ 10 km s^{-1}. The momentum of matter compacting onto the base of this shell, together with the high luminosity, keeps the shell moving outward. Eventually, the shell begins to overtake the material above it, and another shock front forms at the top of the shell. Figure 24 shows clearly the compact nature of the shell and the convergence of material from above and below the mean trajectory. None of the material in the shell is likely to achieve escape velocity during the present expansion. However, ~ 0.3 percent of the mass of the star above the shell (11 zones) attains escape velocity, the outermost zone having a velocity 1.55 times the local escape velocity when computations were stopped because of the short time-steps required. At this stage, the hydrogen ionization zone had moved in to mass fraction 0.8018 (the hydrogen-burning shell is at mass fraction 0.8015). Although close to the hydrogen shell in mass fraction, the hydrogen ionization zone is situated at 80 $R_\odot$. The base of the neutral shell (which coincides with the lower shock front) is situated at 500 $R_\odot$ at this stage, the mass fraction there being 0.809. If the neutral shell and the faster-moving material below it were completely ejected, there would

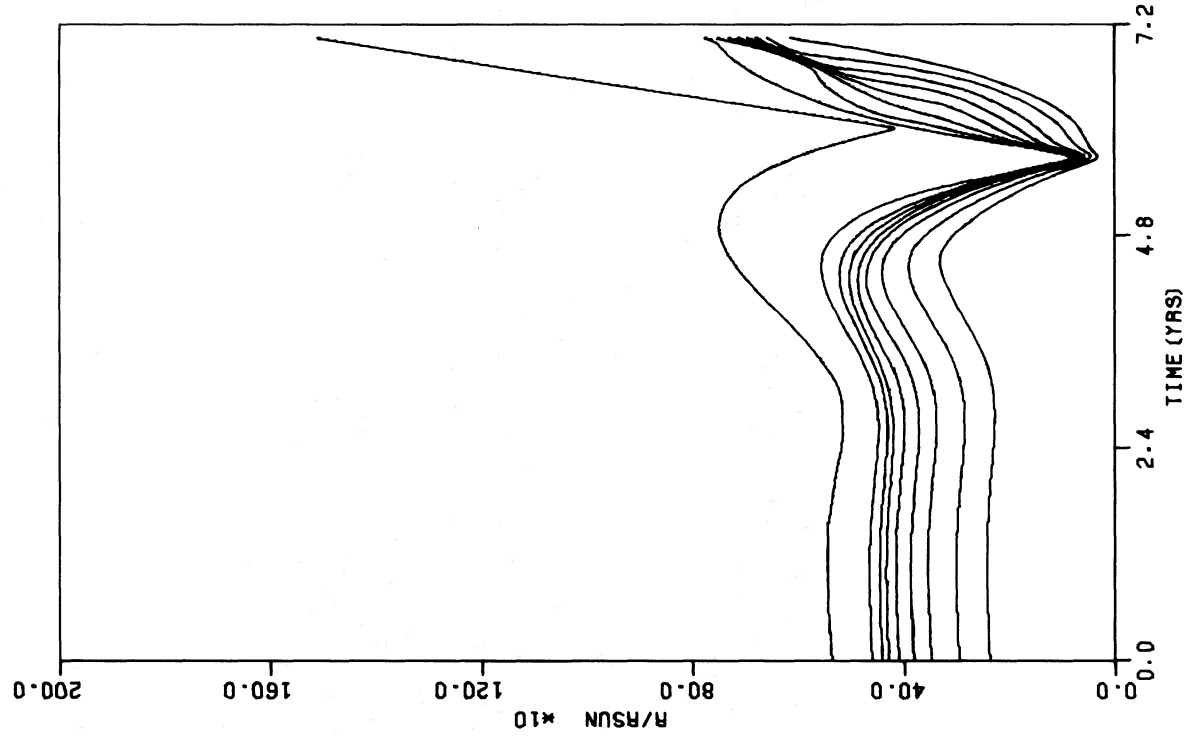

FIG. 24

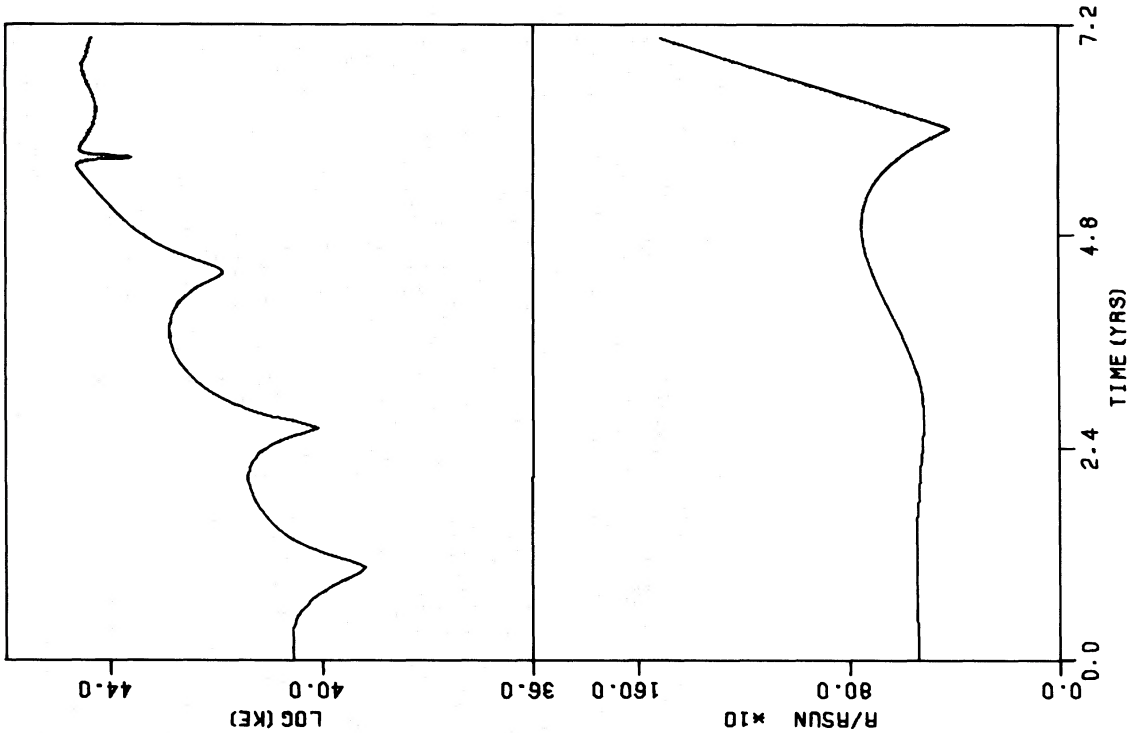

FIG. 23

FIG. 23.—Envelope kinetic energy and surface radius as a function of time in model 14.
FIG. 24.—Radius variation with time in model 4 for points at mass fractions 0.9992, 0.9753, 0.9493, 0.9256, 0.8995, 0.8740, 0.8501, 0.8254, and 0.8096.

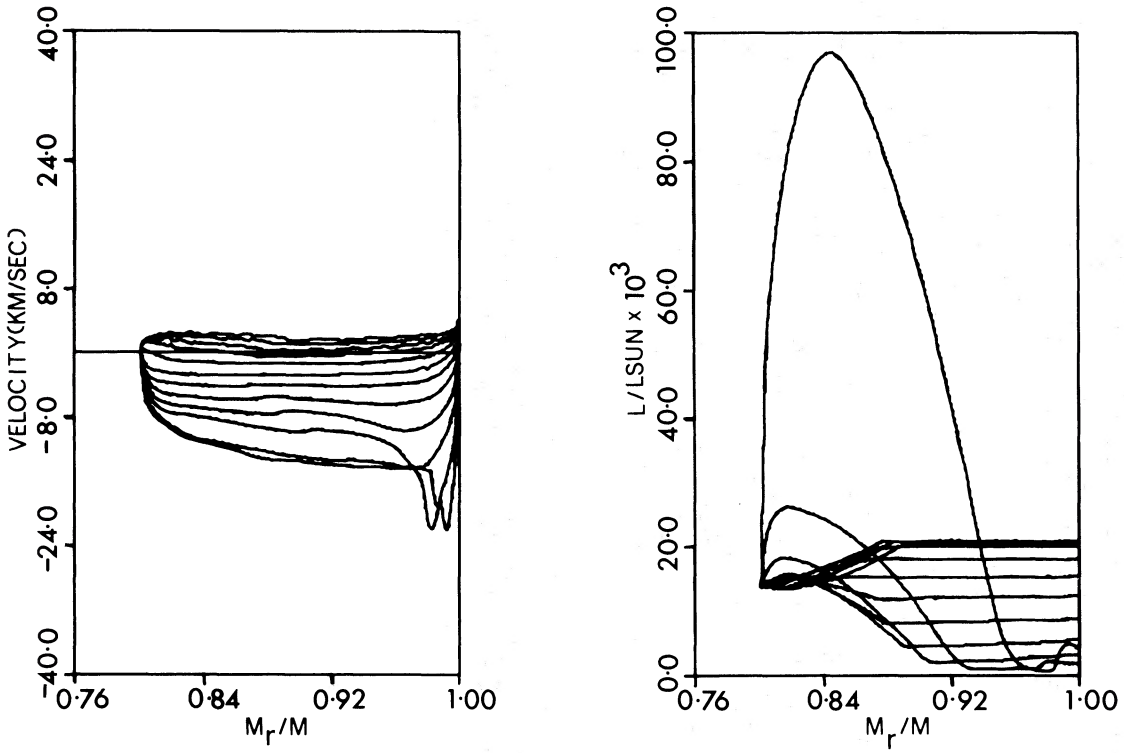

FIG. 25*a* (*left*).—Velocity as a function of mass in model 4 at 0.152-year time intervals during the expansion and collapse phases.

FIG. 25*b* (*right*).—Luminosity profiles corresponding with the velocity profiles in fig. 25*a*. The large interior luminosity occurs during collapse reversal.

be very little hydrogen left on the surface of the remnant star.

With the typical opacities ($\kappa \approx 2 \times 10^{-4}$ cm^2 g^{-1}) in the neutral shell, a luminosity of $\sim 9 \times 10^7 L_\odot$ would be required for ejection by radiation pressure. Since such luminosities are not produced on the giant branch by low-mass stars, the shell must receive sufficient kinetic energy to escape while it is still largely ionized (i.e., in the early rebound stage) if ejection is to occur. Faulkner (1970) and Sparks and Kutter (1972) have produced models for gentle shell ejection via radiation pressure using electron-scattering opacities. These opacities are much larger than those in the shell of neutral material which is found in this model after the rebound.

It was shown in § II(*a*) that the total energy of the static envelope of model 4 is positive and that the efficient conversion of the envelope energy to kinetic energy would be sufficient to eject the envelope with a velocity at infinity of ~ 20 km s^{-1}. However, the dynamical calculations described above show that nonadiabatic effects are sufficient to prevent envelope ejection by a significant margin.

b) *Comparison with Observations*

The formation in model 4 of a distinct outward-moving shell with very little hydrogen-rich material interior to it suggests an association with planetary-nebula ejection. The increase in the velocity of the shell from ~ 3 km s^{-1} in model 3 to ~ 10 km s^{-1} in model 4 indicates that although the shell did not reach escape velocity in the present calculations, higher luminosities may lead to complete shell ejection. Since a given luminosity on the AGB will be reached first when the helium-burning shell is undergoing a thermal instability, ejection will probably occur during such an instability. The time required to complete a shell ejection via an envelope relaxation oscillation will be much shorter than the duration of the luminosity increase resulting from a helium-shell thermal instability (see Schwarzschild and Härm 1967 and Sweigart 1971 for the time scale of shell instabilities).

It was mentioned in § IV(*b*) that all but $\sim 2 \times 10^{-3}$ $M_\odot$ of envelope material must be removed in planetary-nebula ejection. Small amounts of mass loss from the surface layers, as found in this model and also by Keeley (1970*b*) and Smith and Rose (1972), could produce a planetary nebula only over many relaxation cycles if violent relaxation oscillations can be maintained as the envelope mass decreases. No dynamical models with low envelope mass have been studied to test this point.

The symbiotic stars have often been suggested as the precursors of planetary nebulae (O'Dell 1966; Abell and Goldreich 1966 and references therein), mainly because of the appearance of forbidden transition lines in their spectra. The calculations presented here for

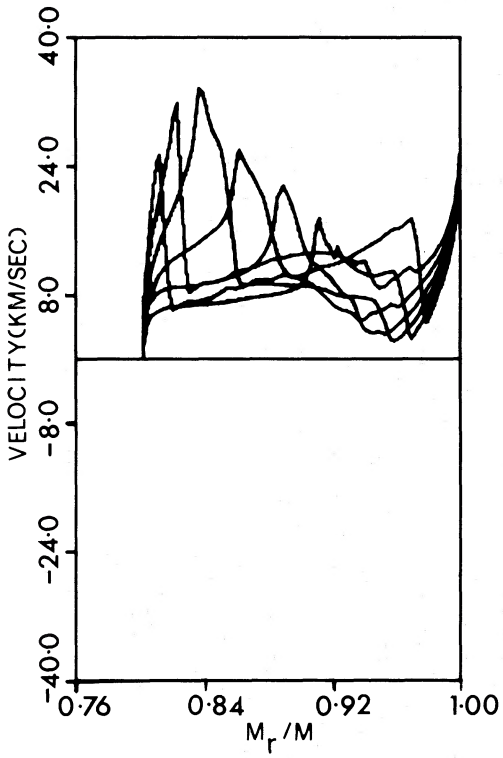

FIG. 26.—Velocity as a function of mass fraction in model 4 at 0.152-year time intervals following the rebound. Shock fronts at the top and base of the outward-moving shell of neutral material are clearly seen. The shock front at the base of the shell moves inward in mass with time while the shock front at the top of the shell moves outward.

models 3 and 4 provide a clearer understanding of the connection between the symbiotic stars and planetary nebulae.

VII. SENSITIVITY OF THE RESULTS TO THE CONVECTIVE TREATMENT

As mentioned in the Appendix, models 1 and 2 used a treatment of time dependence and space averaging of convection which is different from that used in models 3 and 4. To test the sensitivity of the envelope dynamics to changes in the treatment of convection, model 1 was rerun with the treatment used in models 3 and 4. The resulting behavior is shown in figure 27. Convergence difficulties stopped the calculations on this model before mass loss occurred or an equilibrium amplitude was reached. Although changing the treatment of convection caused the periods to change by about 10 percent, the most significant result is the change in the full amplitude mode of pulsation from first overtone to fundamental. The luminosity ($\log L/L_\odot \sim 3.6$) at which the transition from first overtone to fundamental pulsation was found to occur in this study cannot therefore be regarded as very accurate.

VIII. SUMMARY AND DISCUSSION

The dynamical properties of the four models are summarized in table 2. It has been shown that AGB stars of mass 0.9 $M_\odot$ and luminosity $\log L/L_\odot \lesssim 3.6$ pulsate in the first-overtone mode. A comparison of a theoretical first-overtone model with a Mira variable of similar period shows good agreement between the magnitude and phase of the light and velocity curves. The emission lines observed in Miras can be associated with a shock front near the surface of the model. At $\log L/L_\odot \gtrsim 3.60$ on the AGB, the models pulsate in the fundamental mode while simultaneously undergoing envelope relaxation oscillations. This behavior is suggested as an explanation of the properties of some of the symbiotic stars and as the means of production of planetary nebulae. The calculations further show that fundamental pulsation in red-giant stars with realistic core masses is *always* associated with violent relaxation oscillations in the envelope. It can therefore be concluded that the steadily pulsating Mira variables must be first (or higher) overtone pulsators. As previously noted by Keeley (1970*a*) and Langer (1971), the fundamental periods of theoretical models are far too long to explain the periods of the bulk of the Mira variables. Overall, the results indicate that an AGB star will evolve through a phase as a Mira variable, then through a phase as a symbiotic star, and finally it will eject its envelope to produce a planetary nebula.

Variations in the treatment of convection are found to affect the full amplitude mode of oscillation of model 1, although the periods are not greatly altered. Consequently the luminosity at which the transition from first-overtone to fundamental pulsation occurred in this study may not accurately match the transition luminosity for real stars. If it is assumed that a red-giant star that has reached a sufficiently high luminosity to pulsate in the fundamental mode will no longer be recognized as a Mira variable, the observed luminosities of the Mira variables can be used to put a lower limit on the transition luminosity. The data of Osvalds

TABLE 2

PARAMETERS OF THE DYNAMICAL MODELS

Parameter	Model 1	Model 2	Model 3	Model 4
$\log P_I$	12.266	13.131	12.715	11.421
$\log T_I$	6.760	6.759	6.705	6.442
$R_I/R_\odot$	0.290	0.284	0.298	0.385
$\log L/L_\odot$	3.415	3.604	3.846	4.142
$R_{surf}/R_\odot$	250	310	425	536
M_{surf}/M	0.9995	0.9995	0.9995	0.9992
$\delta \log P_I$	0.003	0.03	0.12	0.26
$\delta \log T_I$	0.0008	0.0075	0.027	0.065
P_0 (days)	482	783	1518	1226
Q_0 (days)	0.116	0.136	0.164	0.0937
τ_0 (years)	1.49	3.02	0.44	0.98
P_1 (days)	146	196	...	...
Q_1 (days)	0.035	0.034	...	...
Number of zones	123	153	156	220

NOTE.—Subscript I signifies that the quantity is evaluated at the inner boundary. The quantities $\delta \log P_I$ and $\delta \log T_I$ are the variations in $\log P$ and $\log T$ at the inner boundary during pulsation. M_{surf}/M is the mass fraction at which the outer boundary conditions are applied, and R_{surf} is the radius at the outermost point. The growth rates of pulsation (τ) are obtained from the plots of kinetic energy against time.

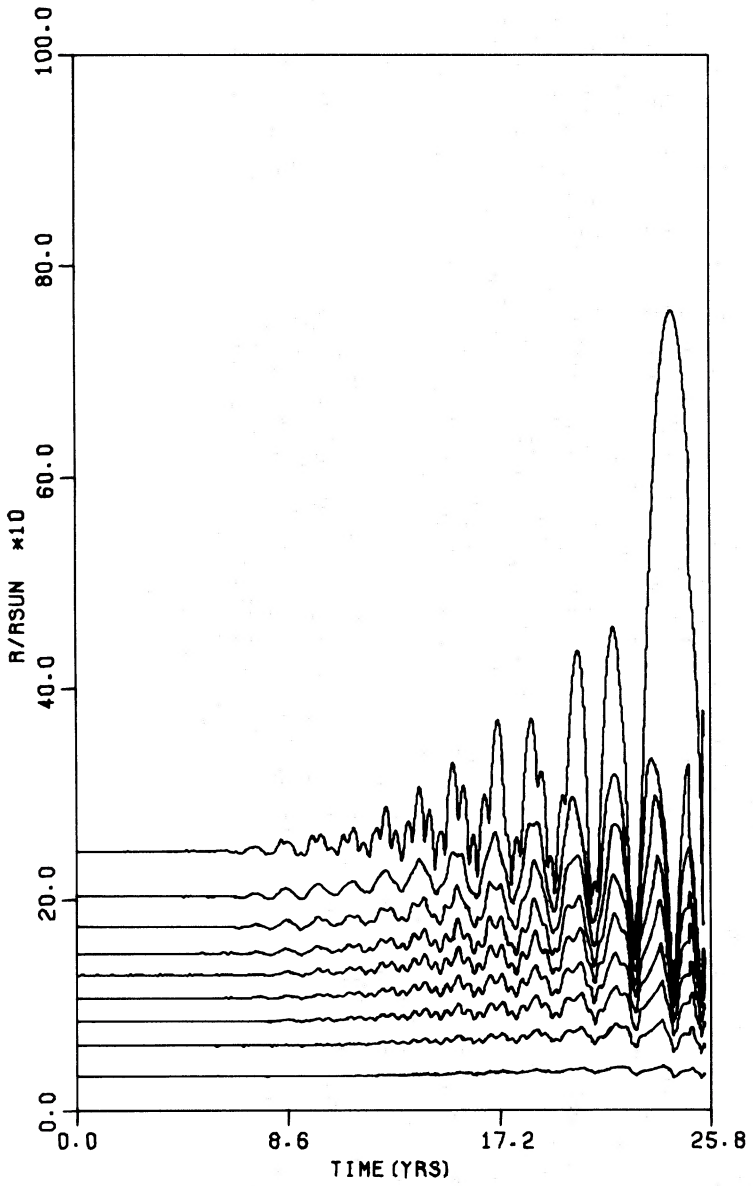

FIG. 27.—Radius variation with time in model 1 when the treatment of convection used in models 3 and 4 is assumed

and Risley (1961), together with the bolometric corrections of Smak (1966) and the amplitude of the bolometric variations given by Pettit and Nicholson (1933), indicate that some Mira variables have luminosities $\log L/L_\odot \gtrsim 4.0$. Thus the transition luminosity estimated in this study ($\log L/L_\odot \sim 3.6$) is considerably lower than the transition luminosity of many observed Mira variables.

A significantly higher transition luminosity could probably be produced by an increase in the total stellar mass. The galactic distribution of Mira variables, which is similar to that of the planetary nebulae (Feast 1972), suggests that they have masses $\sim 1.2\ M_\odot$. Since the core mass is almost independent of the total mass at a given luminosity on the AGB, a $1.2\ M_\odot$ AGB star will have more than twice the envelope mass of any of the four $0.9\ M_\odot$ models produced here. Table 3 shows that increasing the total envelope mass with a constant core mass (and hence luminosity) decreases the fraction of the mass of the envelope above the convection zone without increasing the radius significantly when $M_{\rm env}/M \gtrsim 0.15$. As the driving of pulsation occurs at the outer edge of the convection zone, a smaller mass fraction above the convection zone will favor driving of the overtone mode and lead to the relatively stable pulsation found in Mira variables. Increasing the total stellar mass from $0.9\ M_\odot$ to $1.2\ M_\odot$ should thus result in a significant increase in the transition luminosity.

There is strong evidence that severe mass loss in Population II stars occurs at much lower luminosities than $\log L/L_\odot \sim 4.0$. Feast (1965) has pointed out

TABLE 3

EFFECT OF MASS LOSS ON STATIC ENVELOPE STRUCTURE

M_{env}/M	$M_{above\ conv.\ zone}/M_{env}$	log T_{eff}	log $R/R_\odot$
0.30.....	0.090	3.425	2.481
0.25.....	0.107	3.429	2.473
0.20.....	0.135	3.434	2.464
0.15.....	0.168	3.442	2.448
0.10.....	0.194	3.462	2.409
0.04.....	0.245	3.508	2.3178
0.025.....	0.268	3.529	2.2748

NOTE.—Envelope mass, mass above the convection zone as a fraction of the envelope mass, log T_{eff}, and log $R/R_\odot$ for static models obtained by removing mass from the envelope of model 2, keeping the core mass and luminosity constant.

that no long-period variable with a period longer than 220 days is known in a globular cluster. If it is assumed that the Population II red variables of longest period are also the most luminous, the 192-day variable in 47 Tucanae is one of the most luminous globular-cluster giants. Eggen (1972*a*) finds $\log L/L_\odot = 3.53$ for this variable. The lack of more luminous red variables in globular clusters must result from mass loss. Further evidence for mass loss in Population II giants is the apparent loss of 0.2 $M_\odot$ on the first giant branch at luminosities $\log L/L_\odot \lesssim 3.4$ which was mentioned in § IV. If mass loss in Population II giants is the result of pulsation in the fundamental mode, the transition luminosity in Population II giants must be considerably smaller than for old disk giants. The difference in transition luminosity could result from the smaller initial total mass (and hence envelope mass at a given luminosity) of Population II stars.

I wish to thank Dr. D. J. Faulkner for his continual advice and encouragement. Informative discussions with Professor O. J. Eggen and Drs. M. S. Bessell, A. R. Hyland, A. W. Rodgers, and R. S. Stobie are gratefully acknowledged. During the course of this work I was maintained financially by a Commonwealth Postgraduate Award for which I am grateful.

APPENDIX

I. PHYSICAL ASSUMPTIONS AND NUMERICAL TECHNIQUES

The difference equations used for the hydrodynamic calculations reported here are those of Fraley (1968). It was found that hydrostatic solutions of these difference equations could not be produced in high-luminosity models if the inner boundary conditions were applied close to the core. Therefore, a complete stellar model containing hydrogen and helium-burning shells was obtained with another set of difference equations and the envelope of this model was transferred to the hydrodynamic program together with the mass, radius, and luminosity of the core. The envelope was converged again to hydrostatic equilibrium before being perturbed and followed dynamically.

II. BOUNDARY CONDITIONS

At the inner boundary, the radius and luminosity were assumed constant throughout the calculations. Table 2 shows the variation of the pressure and temperature at the innermost point of each model and the radius at the inner boundary. Since this radius is very small compared with the mean envelope radius, even during collapse phases, it is unlikely that the assumption of constant radius at the inner boundary will cause large errors in the dynamical behavior of the envelope. However, changes in the temperature and pressure in the shell-burning region could result in a change in the luminosity of the core. To check the accuracy of the inner boundary conditions, the two burning shells were included in the dynamical calculations for 0.22 years at the peak of the envelope collapse of model 4. The resulting envelope behavior was identical to that found with the radius and luminosity kept constant at the base of the envelope. In particular, variations in the luminosity of the burning shells were found to be insignificant ($\delta \log L_H/L_\odot \sim 0.0035$, $\delta \log L_{He}/L_\odot \sim 6 \times 10^{-5}$) on the dynamical time scale of the envelope. However, long-term variations (i.e., on a time scale longer than the thermal diffusion time from the burning shells to the envelope) in the core luminosity could be produced by an alteration of the mean temperature structure as a result of pulsation.

The outer boundary conditions were applied at a small mass fraction below the surface of the star. At the surface, it was assumed that $P_{gas} = 0$ and $L = 8\pi\sigma R^2 T^4$ (Chandrasekhar 1934; Kosirev 1934). By further assuming that the diffusion equation is valid and $\rho \propto r^{-2}$, $g_{eff} \propto r^{-2}$, and the opacity is constant above the outermost point in the model, two outer boundary conditions at a fixed mass fraction can be derived. These are

$$\frac{L}{8\pi\sigma R^2} - T^4 = \frac{L\kappa\rho r^2}{16\pi\sigma}\left(\frac{1}{R^3} - \frac{1}{r^3}\right)$$

and

$$\frac{L}{6\pi c R^2} - P = \tfrac{1}{3} g_{eff}\rho r^4\left(\frac{1}{R^3} - \frac{1}{r^3}\right),$$

where

$$R = r + \frac{\delta M}{4\pi\rho r^2}$$

and δM is the mass above the surface point.

III. EQUATION OF STATE

In the coolest parts of the envelope, it is assumed that hydrogen exists in the states H_2, H, and H^+, and that helium and metals are un-ionized. The total

pressure is then made up of contributions from the previously mentioned atoms, ions, and molecules together with a contribution from radiation and electrons. Dissociation of the H_2 molecules is taken from the work of Vardya (1965).

At higher temperatures, the effect of H_2 molecules becomes insignificant and a gas consisting of hydrogen and helium in the states H, H^+, He, He^+, and He^{++} is assumed. Thermodynamics of the gas, together with a contribution from radiation, are treated according to Baerentzen (1965).

The effect of turbulent pressure was not included in the calculations.

IV. OPACITY

The opacity is found by interpolation in the tables of Cox and Stewart (1970). Twelve points of the grid in the $(\log \rho, \log T)$-plane are used in the interpolation procedure to obtain a smooth fit to the opacity.

A contribution to the opacity from water molecules was included according to the simple formula of Paczyński (1969).

V. CONVECTION

The time-independent convective gradient was calculated from the mixing-length theory, using the solution given by Kippenhahn, Weigert, and Hofmeister (1967). In the two lowest-luminosity models, time dependence of convection was included by allowing the convective velocity to vary on a characteristic time scale τ, so that the convective velocity at time t^{n+1} is given by

$$v = v^n + \frac{\delta t}{\tau}(v_0 - v^n), \tag{1}$$

where v_0 is the convective velocity according to the instantaneous mixing-length theory. The time scale τ is taken from the formulation of time-dependence given by Arnett (1969), who requires that

$$\dot{v} = 2\frac{(v_0^2 - v^2)}{l_m}. \tag{2}$$

Equation (2) is approximately satisfied by equation (1) if

$$\tau = \frac{l_m}{2(v_0 + v^n)}, \tag{3}$$

where l_m is the mixing length which is taken as 1 pressure scale-height in these calculations. The convective velocity is allowed to decay via equation (1) and is set to zero when $|\nabla - \nabla_{\rm rad}| < 10^{-6}\nabla_{\rm rad}$.

The coupling between convective elements at adjacent points was included by defining a space-averaged convective velocity

$$v_j' = \alpha_1 v_{j-1}^n + (1 - \alpha_1 - \alpha_2)v_j + \alpha_2 v_{j+1}^n, \tag{4}$$

where

$$\alpha_1 = \tfrac{1}{3}\max\left[0, 1 - \frac{r_j^n - r_{j-1}^n}{l_m}\right],$$

$$\alpha_2 = \tfrac{1}{3}\max\left[0, 1 - \frac{r_{j+1}^n - r_j^n}{l_m}\right].$$

Keeley (1970*b*) treated nonlocal convection by averaging convective luminosity rather than convective velocity over adjacent points.

In the earlier calculations involving the two high-luminosity models, τ was defined by $\tau = l_m/v$. Space averaging of convection was included as above except that v_{j-1}^n and v_{j+1}^n in equation (4) were replaced by v'^n_{j-1} and v'^n_{j+1}, respectively, while v^n in equation (1) was replaced by v_n'. The disadvantage of this earlier formulation of nonlocal convection is that the edge of a convective region can expand via space averaging without restriction by the local growth rate.

Given the convective velocity v', the convective temperature gradient ∇ according to the mixing-length theory is given by

$$\nabla = \frac{\nabla_{\rm rad} + \beta\nabla_{\rm ad}}{1 + \beta},$$

where

$$\beta = \frac{9}{4}\frac{\Gamma^2}{(1 + \Gamma)} \quad \text{and} \quad \Gamma = \frac{C_p\kappa\rho^2 l_m v'}{6acT^3},$$

and Γ is known as the convective efficiency (Cox and Giuli 1968).

It is worthwhile noting that the treatment of time dependence of convection given by Cox, Brownlee, and Eilers (1966), where the convective flux or luminosity rather than the convective velocity is allowed to vary on a convective time scale, was found to be unsatisfactory because it led to convergence difficulties in the high-luminosity models.

VI. ENERGY CONSERVATION

For a star with $N - 1$ zones, the difference equations of Fraley give rise to the conservation equation

$$E - E^n = [\textstyle\sum_{j=1}^{N-1}\delta M_{j+1/2}\epsilon_{j+1/2} - L + L_I](t - t^n) - 4\pi\langle r_N^2\rangle\langle P + Q\rangle_{N+1/2}(r_N - r_N^n) - \zeta^n,$$

where

$$\zeta^n = (\theta - \tfrac{1}{2})\textstyle\sum_{j=1}^{N-1}\delta M_{j+1}(v_{j+1} - v_{j+1}^n)^2$$

and other symbols have their usual meaning. Both sides of the conservation equation were evaluated at each time step and found to agree to at least six decimal places. The term ζ^n is a correction term which vanishes if $\theta = 0.5$. However, $\theta = 0.51$ was used for stability reasons as suggested by Fraley so that energy is not exactly conserved. To test the significance of the correction term, the quantity $\xi^n = \sum_n\zeta^n/\sum_n|KE - KE^n|$ was evaluated at each time step for each series of models. It was found that $\xi^n < 2 \times 10^{-3}$ for all models.

REFERENCES

Abell, G. O., and Goldreich, P. 1966, *Pub. A.S.P.*, **78**, 232.
Aller, L. H. 1954, *Astrophysics: Nuclear Transformations, Stellar Interiors and Nebulae* (New York: Ronald Press), p. 180.
Arnett, W. D. 1969, *Ap. and Space Sci.*, **5**, 180.
Baerentzen, J. 1965, *Zs. f. Ap.*, **62**, 221.
Berman, L. 1932, *Pub. A.S.P.*, **44**, 318.
Chandrasekhar, S. 1934, *M.N.R.A.S.*, **94**, 444.
Cox, A. N., Brownlee, R. R., and Eilers, D. D. 1966, *Ap. J.*, **144**, 1024.
Cox, A. N., and Stewart, J. N. 1970, *Ap. J. Suppl.*, **19**, 243.
Cox, J. P., and Giuli, R. T. 1968, *Principles of Stellar Structure*, Vol. **1** (New York: Gordon & Breach).
Demarque, P., and Mengel, J. G. 1972, *Ap. J.*, **171**, 583.
———. 1973, *Astr. and Ap.*, **22**, 121.
Eggen, O. J. 1971*a*, *Ap. J. Suppl.*, **22**, 389.
———. 1971*b*, *Ap. J.*, **163**, 313.
———. 1971*c*, *ibid.*, **165**, 317.
———. 1972*a*, *ibid.*, **172**, 639.
———. 1972*b*, *ibid.*, **177**, 489.
———. 1973, *ibid.*, **180**, 857.
Eggleton, P. 1968, *M.N.R.A.S.*, **140**, 387.
Faraggiana, R., and Hack, M. 1971, *Astr. and Ap.*, **15**, 55.
Faulkner, D. J. 1970, *Ap. J.*, **162**, 513.
———. 1972, *Proc. Astr. Soc. Australia*, **2**, 72.
Faulkner, D. J., and Cannon, R. D. 1973, *Ap. J.*, **180**, 435.
Feast, M. W. 1965, *Observatory*, **85**, 16.
———. 1972, *Quart. J.R.A.S.*, **13**, 191.
Finzi, A., and Wolf, R. A. 1971, *Astr. and Ap.*, **11**, 418.
Fraley, G. S. 1968, *Ap. and Space Sci.*, **2**, 96.
Gauzit, J. 1955, *Ann. d'Ap.*, **18**, 354.
Gerola, H., and Panagia, N. 1968, *Ap. and Space Sci.*, **2**, 285.
———. 1970, *ibid.*, **8**, 120.
Glass, I. S., and Feast, M. W. 1973, *M.N.R.A.S.*, **163**, 245.
Hain, D. D. 1969, thesis, Australian National University (many of the results in this thesis are published in D. Shinkawa, 1973, *Ap. J. Suppl.*, No. 218, **25**, 253).
Hogg, F. S. 1934, *Pub. AAS*, **8**, 14.
Hoyle, F. 1956, *Ap. J.*, **124**, 482.
Hyland, A. R., Becklin, E. E., and Neugebauer, G. 1972, *Astr. and Ap.*, **16**, 204.
Iben, I. 1968, *Ap. J.*, **154**, 581.
Iben, I., and Rood, R. T. 1970, *Ap. J.*, **161**, 587.
Kamijo, F. 1962, *Pub. Astr. Soc. Japan*, **14**, 271.
Keeley, D. A. 1970*a*, *Ap. J.*, **161**, 643.
———. 1970*b*, *ibid.*, **161**, 657.
———. 1970*c*, thesis, California Institute of Technology.
Kippenhahn, R., Weigert, A., and Hofmeister, E. 1967, *Methods in Computational Physics*, Vol. 7 (New York: Academic Press), p. 129.
Kosirev, N. A. 1934, *M.N.R.A.S.*, **94**, 430.
Langer, G. E. 1971, *M.N.R.A.S.*, **155**, 199.
Merrill, P. W. 1960, *Stellar Atmospheres*, ed. J. L. Greenstein (Chicago: University of Chicago Press), p. 509.
O'Dell, C. R. 1966, *Ap. J.*, **145**, 487.
Osterbrock, D. E. 1964, *Ann. Rev. Astr. and Ap.*, **2**, 95.
Osvalds, V., and Risley, A. M. 1961, *Pub. Leander McCormick Obs.*, **11**, part 21, 147.
Paczyński, B. 1969, *Acta Astr.*, **19**, 1.
———. 1970, *ibid.*, **20**, 47.
Paczyński, B., and Ziołkowski, J. 1968, *Acta Astr.*, **18**, 255.
Payne-Gaposhkin, C. 1964, *The Galactic Novae* (New York: Dover), p. 306.
Pettit, E., and Nicholson, S. B. 1933, *Ap. J.*, **78**, 320.
Rood, R. T. 1972, *Ap. J.*, **177**, 681.
Rose, W. K., and Smith, R. L. 1970, *Ap. J.*, **159**, 903.
Roxburgh, I. W. 1967, *Nature*, **215**, 838.
Sahade, J. 1960, *Stellar Atmospheres*, ed. J. L. Greenstein (Chicago: University of Chicago Press), p. 494.
Salpeter, E. E. 1971, *Ann. Rev. Astr. and Ap.*, **9**, 127.
Schwarzschild, M. 1948, *Ap. J.*, **107**, 1.
Schwarzschild, M., and Härm, R. 1967, *Ap. J.*, **150**, 961.
Smak, J. 1964, *Ap. J. Suppl.*, **9**, 141.
———. 1966, *Ann. Rev. Astr. and Ap.*, **4**, 19.
Smith, R. L., and Rose, W. K. 1972, *Ap. J.*, **176**, 395.
Sobolev, V. V. 1960, *Moving Envelopes of Stars* (Cambridge: University of Chicago Press).
Sparks, W. M., and Kutter, G. S. 1972, *Ap. J.*, **175**, 707.
Sweigart, A. V. 1971, *Ap. J.*, **168**, 79.
Vardya, M. S. 1965, *M.N.R.A.S.*, **129**, 205.
Wisse, M., and Wisse, P. N. J. 1971, *Astr. and Ap.*, **12**, 143.